ABSTRACT

Title of Thesis: CHARACTERIZATION OF IRON OXIDE NANOPARTICLES IN STRUCTURAL SILK-ELASTINLIKE PROTEIN POLYMER

Jennifer Shih, Master of Science, 2012

Directed By: Robert M. Briber

Department of Materials Science and Engineering

The structure of silk elastin-like protein (SELP) block copolymers containing Fe_3O_4 magnetic nanoparticles are investigated. These materials have potential applications for hyperthermia cancer therapy. SELPs undergo a gel transition at physiological temperatures, which can be used to localize delivery of nanoparticles at tumor sites. Vibrating sample magnetometry (VSM), transmission electron microscopy (TEM), and small angle neutron scattering (SANS) are used to characterize the nanoparticles and the SELP-nanoparticle nanocomposite system. A series of nanoparticles with three different nominal diameters, 30, 50 and 80 nm, were added to 4 and 8 wt.% SELP samples. Different functionalities on the nanoparticle surface affect their interactions with SELP. The 50 nm nanoparticles in SELP exhibit chaining (linear association of the nanoparticles), while the 30 nm nanoparticles are too small and settle out of the polymer mesh and the 80 nm nanoparticles tend to cluster without any regard for SELP structure. The SELP concentration does not have a major affect on nanoparticle behavior in the nanocomposites.

CHARACTERIZATION OF IRON OXIDE NANOPARTICLES IN STRUCTURAL SILK-ELASTINLIKE PROTEIN POLYMER

By

Jennifer Shih

Thesis submitted to the Faculty of the Graduate School of the
University of Maryland, College Park in partial fulfillment
of the requirements for the degree of
Masters of Science
2012

Advisory Committee:

Professor R.M. Briber (Chair)
Dr. J.A. Borchers
Dr. C.L. Dennis
Professor J. Seog

Acknowledgements

I would like to thank the many people that have supported me and given me guidance throughout the completion of my thesis. Thank you to my advisors from UMD and NIST, Prof. Robert Briber, Dr. Cindi Dennis and Dr. Julie Borchers. Your feedback and guidance over the course of my research has been invaluable. Also to Julie and Cindi for supporting me ever since I first met them as an undergraduate summer intern at NIST. I would also like to thank the fourth member of my thesis committee, Prof. Joonil Seog, for his time and review of my work.

Thank you to everyone who has helped me with any aspect of my project, Von Cresce of the Army Research Laboratory, Dr. Wen-An Chiou and Larry Lai of the NISP Lab, Dr. Andrew Jackson of NIST for his neutron scattering expertise, Sean Fackler and Huong Vu with VSM measurements, among many others.

I lastly want to thank my friends and family. Thank you for all the phone calls, Skype calls, Starbucks work sessions, words of support and encouragement and well-meaning distractions. I couldn't have done without any of it and I'm so grateful!

Table of Contents

List of Tables

List of Figures

Chapter 1

1.1 Introduction

The potential use of magnetic nanoparticles to selectively kill cancer cells through hyperthermia therapy is a topic that is being extensively studied. When an external alternating magnetic field (AMF) is applied to magnetic nanoparticles, they generate heat from several possible mechanisms, which is measured as a specific absorption rate (SAR). Once the temperature reaches 42°-45°C at the tumor site, necrosis of the tumor cells can occur locally without harming the surrounding healthy tissue. After the application, the nanoparticles can pass through the body without harmful effects if the material is biocompatible[1]. Researchers have been investigating ways to uniformly deliver heat to treat a tumor deep within a patient since the idea was first published in 1957 by Gilchrist, et al.[2] for the treatment of lymphatic metastases. Hyperthermia therapy offers many possible benefits over traditional cancer treatments such as radiotherapy and chemotherapy. The number of repeat treatments allowed is greater since the risk of toxic side effects is lower and the procedure is minimally invasive. Also, it has been proven that even slightly elevated temperatures of particles through hyperthermia can increase the potency of other treatments[3]. Current therapies propose many different ways to use nanoparticles, with the ultimate goal of hyperthermia therapy being functionalized smart nanoparticles with receptors that find tumors by themselves[4–7]. However, the focus of this research is on the short-term goal of directly injecting nanoparticles into a tumor site for hyperthermia treatment. The main problem with this method is controlling the dispersion of the nanoparticles after injection. Freely moving nanoparticles could invade neighboring healthy organs or be taken up by the arteries and transported elsewhere[3].

Thus, an immobilization process is needed to keep the nanoparticles at the tumor site. The addition of a biocompatible and degradable polymer to the nanoparticles has the potential to create a functional hyperthermia cancer treatment process. Nanoparticles will remain at the tumor site without invading healthy tissue and can be uniformly distributed, improving uniformity of temperature elevation and thus, increasing the overall effectiveness of the hyperthermia treatment. Also, depending on polymer degradation time, multiple treatments can be applied with only one injection[3]. Dextran coated magnetite (Fe_3O_4) nanoparticles when combined with silk-elastinlike protein (SELP) polymer, form a nanocomposite system that stabilizes injected nanoparticles at a localized tumor site for hyperthermia therapy. In this thesis, structural and magnetic characterization of the nanoparticle/SELP nanocomposite system were completed in order to further the understanding of the properties of this system and their interactions. Transmission Electron Microscopy (TEM) and Small Angle Neutron Scattering (SANS) give structural information, while Vibrating Sample Magnetometer (VSM) measurements offer insight into the magnetic behavior of the system. The interaction behavior of the nanoparticles in SELP affects their structural alignment within the SELP gel and potentially the amount of heat generated in a magnetic field.

1.2 Iron oxide nanoparticles

The nanoparticles in the system are dextran coated Fe_3O_4, magnetite, particles that exhibit a core shell structure. The core is comprised of Fe_3O_4, while the shell is a dextran layer. A schematic of the structure of the nanoparticles is shown in figure 1.1 below[1].

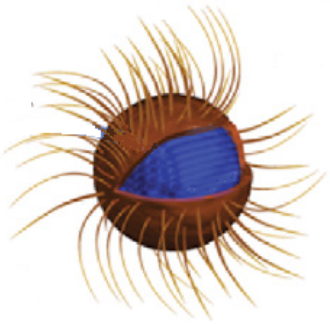

Figure 1.1 Dextran coated Fe_3O_4 nanoparticles

Previous measurements from electron beam diffraction suggest that the cores are crystallographically oriented in one primary direction, with at most one secondary orientation. Fe_3O_4 is often chosen for biomedical applications because it exhibits low toxicity while also maintaining useful magnetic properties. The dextran coating reduces nanoparticle aggregation by inducing interparticle repulsion yet still allows for collective magnetic behavior of the nanoparticles. Dextran can also potentially enhance interactions with biological molecules and has a molecular weight of 40 kilodaltons[1,8,9]. The nanoparticles were manufactured in collaboration with Cordula Gruettner at Micromod Partikeltechnologie, GmbH. They were synthesized by a high temperature, high pressure homogenization and the dextran coating was physically adsorbed onto the surface to create a single dextran layer[10]. Physisorption relies on weak van der Waals bonds, which is in contrast to chemisorption, where covalent and ionic bonds are created between the surface and the attachment. Some samples were synthesized to have a double dextran layer, meaning that the number of attachments to the particle surface doubles, instead of the creation of a second dextran layer on top of the first. Single dextran coated nanoparticles were coated a second time at high temperature, but different pressure conditions to achieve a double dextran layer. Additional samples also included functional surface groups such as amine (NH_2) or maleimide ($H_2C_2(CO)_2NH$) added to the double

dextran layer. Amine was added because it is a required processing step to create maleimide. The maleimide coating was created because it will eventually be used as an attachment for targeting moieties on the nanoparticles. These functionalities can be characterized to determine their effect on nanoparticle stabilization and aggregations[11]. Nanoparticles of three different sizes, 30, 50 and 80 nm hydrodynamic diameter as measured using dynamic light scattering by Micromod were investigated.

1.3 Silk Elastin-Like Polymer

Silk elastin-like polymer, SELP 47K, which contains four silk units, seven elastin units and a lysine (K) modified elastin, is useful for biomedical applications because it undergoes a sol/gel transition temperature at 37°C. This transition temperature corresponds to physiological temperature, which makes it ideal for localized hyperthermia cancer therapy. The polymer will gel after it has been injected into the body, thus stabilizing the nanoparticles at the tumor site. SELP polymer has a block copolypeptide structure of alternating silk (GAGAGS) from *Bombyx mori* (silkworm) and mammalian elastin (GVGVP) blocks, with a lysine substituted elastin unit (GKGVP)[12] as seen in Figure 1.2.

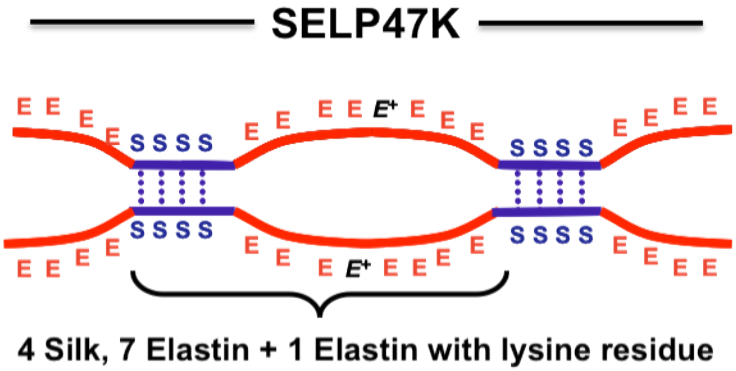

Figure 1.2 Structure of SELP 47K

The entire amino acid sequence for SELP 47K is as follows:

MDPVVLQRRDWENPGVTQLVRLAAHPPFASDPMGAGSGAGS[(GVGVP)$_4$GKGV P(GVGVP)$_3$(GAGAGS)$_4$]$_{12}$(GVGVP)$_4$GKGVP(GVGVP)$_2$(GAGAGS)$_2$GAGAMDPGRY QDLRSHHHHHH. SELP 47K has a molecular weight of 69,814 Da[13]. The dispersion of "hard" blocks and "soft" blocks in a polymer chain allow multiple cross-links to form across many polymer chains. The crystallization of the silk, as well as the lysine unit in the elastin block, allow gelation to occur[14]. SELP self-assembles due to intermolecular interactions such as hydrogen bonding, hydrophobic interactions and electrostatic interactions[12]. Figure 1.3 is an transmission electron microscopy image taken of SELP 47K[15] embedded in epoxy. The multiple cross-links created and internal fibrillar structure of the polymer can be observed.

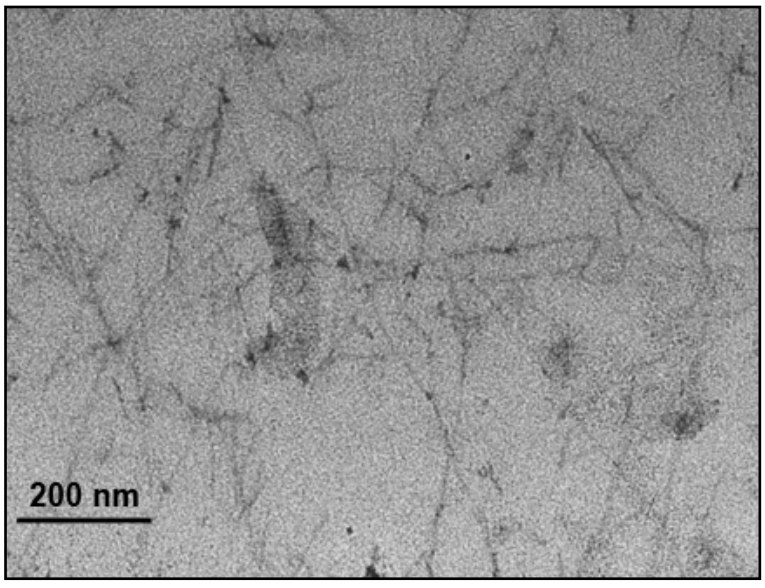

Figure 1.3 Transmission electron microscopy image of SELP 47K

SELP was synthesized through gene expression of cells by Joe Cappello at Protein Polymer Technologies, Inc. Silk provides mechanical stability and crystallinity, while

elastin has aqueous solubility[16] By altering the chemical structure of SELP, other properties can be modified, such as temperature, ionic strength and pH sensitive swelling[15]. For SELP 47K, the amount of SELP must be between 4 and 12 wt.% in order for gelation to occur. Two weight percentages in this gelation window, 4 and 8 wt.%, will be examined to determine the most effective concentration of SELP 47K to form nanocomposites.

1.4 Nanocomposite System

The inclusion of iron oxide nanoparticles in SELP 47K creates a nanocomposite system that combines the magnetic properties from the nanoparticles needed for heat generation with the structure of the SELP network that provides stabilization for the particles at a targeted tumor site. This nanoparticle/SELP nanocomposite system is cured at 37°C and undergoes a sol/gel transition. The nanocomposite system is biocompatible and contains harmless degradation products.

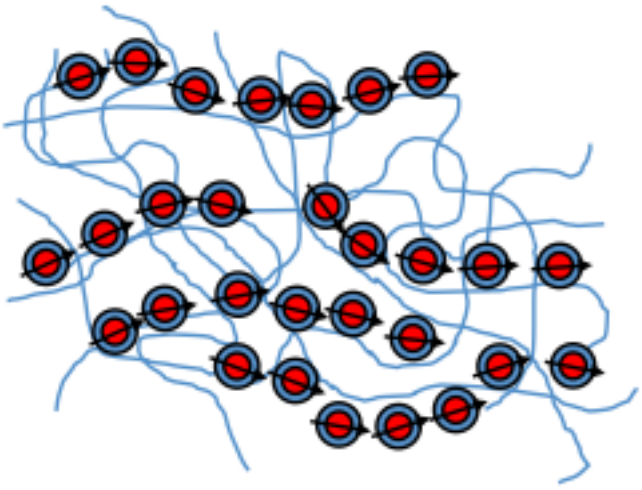

Figure 1.4 Nanoparticle/SELP nanocomposite system

These nanoparticle/SELP nanocomposite systems must be characterized to understand the structural and magnetic properties of the combined system. Important aspects of the structure include the nanoparticle placement within the SELP network and whether the nanoparticles align within the polymer matrix. Ideally, nanoparticles will exhibit chaining behavior and form long chains of nanoparticles that mimic the SELP structure, as shown in the schematic in Figure 1.4 above[16]. The chaining behavior is dependent on the size of the nanoparticles and the surface coating. The nanoparticle surface coatings will have intermolecular interactions with the SELP 47K material, affecting their behavior and if they aggregate or align within the polymer. If the nanoparticles do not exhibit chaining, they are likely to be randomly clustered throughout the SELP, without any regard to the network structure. Another possibility is that the nanoparticles could cluster and precipitate out of SELP. The magnetic properties of the nanoparticles/SELP nanocomposite depend on the chaining behavior of the particles. If chaining is present, then the collective anisotropic behavior is likely to be enhanced. However, if chaining is low or not present, anisotropy will not be evident in the sample. The chaining behavior of the nanoparticles within SELP polymer will affect the heat generation of the nanocomposite system and the overall potential effectiveness of the hyperthermia therapy.

1.5 Prior Research

Extensive research on the magnetite nanoparticles and SELP material can be found separately, but not however as a combined system. Dennis, et al., discuss the success of using dextran coated magnetite nanoparticles for the nearly complete regression of tumors in mice trials. They highlight the importance of collective magnetic behavior in

the kilohertz frequency range, which they found to generate a substantial amount of heat, as measured in Wg^{-1} as specific absorption rate (SAR). Also, the saturation magnetization, anisotropy, relaxation time of the magnetic moments, amplitude and frequency of the external AMF and intratumor particle concentration and distribution are all factors that contribute to the maximum heat dose per amount of material. Heat generation was also found to be dependent on the interactions of nanoparticles, particularly nanoparticle spacing and anisotropy. Dennis, et al. also discuss the possible mechanisms of heat generation being hysteresis, eddy current, Neel paramagnetic switching and friction from Brownian rotation[15]. Ghandehari, et al. at the University of Utah, investigate the synthesis and characterization for the utility of biocompatible SELP polymers as intratumoral gene delivery carriers. They report a high control over the polymer sequence and length of silk and elastin blocks during SELP synthesis. They were able to synthesize and characterize a family of SELP polymers with different combinations of silk and elastin block lengths to demonstrate the ease of control[1]. This allows for manipulation of polymer gelation time, degradation, mechanical strength and other properties indicating the SELP material can be synthesized according to meet the needs of the delivery system or application[17]. Ideally for our studies, the SELP polymer will act as a nanoparticle stabilizer and delivery vehicle.

1.6 Relevant Applications

Hyperthermia cancer therapy is a potential application for the nanoparticle/SELP nanocomposite system studied within this thesis. Dennis, et al. have shown that there is significant heat generation created from the nanoparticles. With the addition of the SELP 47K material, the nanocomposite system may provide a stable structure to locally contain

the nanoparticles. Other relevant biomedical applications include cell labeling and separation, magnetofection (a method for introducing nucleic acids into cells that utilizes magnetic fields) for gene delivery, a delivery vehicle for therapeutics or enhanced contrast for magnetic resonance imaging (MRI)[13,18]. The biggest challenge with cell labeling is the difficulty of accounting for a dilution effect caused by cell division without effecting normal cell function. Human serum albumin coated iron oxide nanoparticles were incubated with several different cell lines to examine the efficiency of cell labeling with nanoparticles. After 24 hours, over 95% of the cell lines were found to be still labeled with the nanoparticles. It is believed that the nanoparticle uptake in cells occurred through endocytosis and phagocytosis or that the human serum albumin coating facilitated cellular uptake through positive interactions with receptors on the cell surface[13,19–21]. Magnetofection is a transfection method that is described as a magnetically enhanced nucleic acid delivery system. The process involves concentrating nucleic acids with cationic magnetic nanoparticles to a targeted cell through an external magnetic field. Experiments thus far have proven a three fold increase in gene delivery efficiency using magnetic nanoparticle magnetofection[21]. Ghandehari, et al., originally examined using the SELP polymer as a delivery vehicle for plasmid DNA and adenoviruses. The swelling, release and degradation properties of SELP make it an ideal therapeutic delivery system, as the rates of each of these properties are highly dependent on polymer concentration and structure[20]. Oleic acid-coated iron oxide nanoparticles are being examined for simultaneously functioning as a drug delivery method and as a contrast agent in MRI. These two applications can be used simultaneously for non-invasive, real-time monitoring of drug delivery to a targeted area using MRI, as well as following the

progression of the effectiveness of the treatment over a prolonged period of time[13]. Magnetic nanoparticles lend themselves to a variety of biomedical applications in addition to hyperthermia therapy and prove to be interesting subjects for further studies continuing to explore the many possibilities.

Chapter 2

Characterization Techniques

2.1 Introduction

A number of characterization techniques were employed to investigate the structural and magnetic properties of the nanoparticles and nanoparticle/SELP nanocomposite system. Dynamic light scattering (DLS), transmission electron microscopy (TEM) and small angle neutron scattering (SANS) provided structural information about the size, shape and crystallinity of our particles. In the nanoparticle/SELP nanocomposite system, TEM and SANS offer insight into how the nanoparticles and SELP interact and how the nanoparticles situate themselves inside the SELP network. Vibrating sample magnetometry (VSM) is used to quantify the magnetic properties of the nanoparticle/SELP nanocomposite system. Collectively, these characterization techniques provide important information on the behavior of the nanocomposite system, which is critical for the intended applications.

2.2 Dynamic Light Scattering

Dynamic light scattering (DLS) measures the approximate size distribution of particles in colloidal suspension that undergoes Brownian motion. DLS was used to obtain initial size measurements of the nanoparticles as sample preparation is simple and measurements can be obtained quickly. Samples are prepared by diluting the concentration of the nanoparticle suspension to 1/100, 1/500 and 1/1000 dilutions. The solutions are then added to a 1µl cuvette with a small window on one wall towards the bottom of the cuvette. This cuvette is then placed in the DLS chamber. Monochromatic light is directed

at and scattered by the particles in the solution. The mean squared displacement, $\langle \Delta r^2 \rangle$, of particles is described by

$$\langle \Delta r^2(\tau) \rangle = 6D_0\tau$$

where D_0 is the particle diffusion coefficient that is defined by the Stokes-Einstein equation and τ is time. The wavelength of the light is altered according to the size of the particle, which is calculated using the Stokes-Einstein equation[19].

$$D_0 = \frac{kT_0}{6\pi\eta R}$$

where k is Boltzmann's constant, T_0 is the sample temperature, η is the solvent viscosity and R is the hydrodynamic radius of the particles in solution[22]. The dextran coat on the nanoparticles most likely expands when in solution, thus increasing the diameter of the nanoparticles measured by DLS as compared to TEM.

2.3 Transmission Electron Microscopy

Transmission electron microscopy (TEM) is a microscopy technique that utilizes electrons to image the structure of a sample at high resolution. Electrons are transmitted or absorbed by the sample. Elements with a lower atomic number, such as organic SELP, have a low z contrast, while elements with a high atomic number, such as iron oxide, will have a greater z-contrast and be easier to image in the TEM. The samples were imaged at the Nanoscale Imaging and Spectroscopy Laboratory (NISP) at the University of Maryland using a JEOL JEM 2100 LaB6 TEM. Nanoparticle suspensions in water and nanoparticle/SELP nanocomposite systems were both examined. Nanoparticle only samples were prepared by placing two to three drops of 1:1000 dilutions onto 3 mm

copper TEM grids covered with a carbon film and allowed to dry on filter paper. TEM imaging revealed large aggregations of nanoparticles and very little dispersion. Nanoparticle/SELP nanocomposite system samples were prepared by first thawing the frozen SELP 47K material. At room temperature the sol/gel transition of the SELP begins. In this experiment, both 4 wt.% and 8 wt.% SELP 47K samples were synthesized. SELP material was pipetted into test tubes. Previously prepared solutions of nanoparticles of different sizes and surface coatings were injected into the same capsule as SELP material and vortex mixed for several seconds to ensure complete dispersion. Samples of the preparation were separated into individual capsules for TEM and VSM and directly into the sample cell for SANS and placed in an oven at 37°C for two hours. Gelation of the SELP is complete under these conditions. The nanoparticle/SELP nanocomposite samples are kept at refrigerated temperatures for storage until needed. The gelled samples were next embedded in a glycol methacrylate (GMA) resin to be suitable for ultramicrotoming. Without embedding the samples, the nanocomposite system is too soft to be ultramicrotomed. GMA resin requires the presence of water in order to cure, however too much water can impede the gelation process. GMA was applied to the capsules that held the nanoparticles with 8 wt.% SELP and cured at 60°C for 24 hours. However, the nanoparticles with 4 wt.% SELP samples required a water/ethanol exchange process before they could be embedded in GMA resin. A portion of the soft gel sample was removed from the capsule and placed onto a piece of filter paper folded into a conical shape. This cone, with the sample sitting down at the tip, was placed into a 50 mL glass beaker. The sample was placed in filter paper for easy removal and capture of all degradation products. 100% H_2O was pipetted into the beaker and filtered through the

paper while the sample sat immersed in the H_2O solution. After one hour, the filter paper with the sample was removed from the beaker, the water was removed, and the sample returned to the beaker. Next, a 3:1 solution of water to ethanol was added to the beaker. This exchange process continued with solutions of 1:1 and 1:3 water to ethanol, each for one hour. Since GMA requires the presence of water, the exchange process was stopped after the 1:3 water to ethanol solution. The nanoparticle/SELP nanocomposite sample was placed into a new capsule and GMA resin was added. These samples were then cured for 60°C for 24 hours. After both the 4 wt.% and 8 wt.% SELP nanocomposite samples were cured, they are cut out of the capsules using a razor blade and ultramicrotomed. Ultramicrotomy is a TEM sample preparation technique that cuts sections less than 100 nm thick which allows electrons to penetrate through the sample for proper TEM imaging. A Leica Microsystems Ultramicrotome was used. The embedded samples were sectioned to be about 100 nm thick using a glass blade and then a diamond blade for precision. The sections are cut and floated onto water. A 3 mm copper TEM grid was carefully dropped onto the floating sections. The TEM grid can then be removed from the waterbed using self-closing tweezers, with the sample section attached. The sample is allowed to air dry to minimize disruption to the sample. After drying, these samples were carbon coated with a carbon sputter coater to prevent charging in the electron microscope. Samples with both nanoparticles and SELP material were imaged at 100 kV to enhance contrast, versus nanoparticle only samples that were imaged at 200 kV.

2.4 Small Angle Neutron Scattering

Small angle neutron scattering (SANS) uses neutrons that are elastically scattered by the atomic nuclei in the sample. The neutron wavelength and the scattering angle dictate the

length scale of the structure that is being probed. The 30 m NG-3 SANS instrument at the NIST Center for Neutron Research (NCNR) can probe structural features between 1 to 500 nm. Neutrons are especially suited for investigating the nanoparticle/SELP nanocomposite systems because they are sensitive to the magnetic moments of the nanoparticles. Thus, SANS can provide information on both the physical structure of the nanocomposite samples as well as the magnetic properties[23]. Ultra small neutron scattering (USANS) can also be used[24] to probe structures of longer length scales on the order of 10^2 to 10^4 nm. The SELP polymer thaws rapidly at room temperature and quickly approaches the sol/gel transition. The preparation of the nanoparticle/SELP polymer nanocomposite needed to occur before the polymer gelled. The SELP is stored in syringes in a -40°C freezer. Once the syringe is removed from the freezer, it is placed in an ice bath until it thaws. This transformation is apparent as the polymer physically changes from translucent to transparent. At this point, nanoparticles are injected into the SELP according to the weight percent of the sample being made. For these experiments, 4 and 8 wt.% samples of SELP were created. A vortex mixer is used on the capsule of nanoparticles and SELP to ensure thorough dispersion of the nanoparticles into the polymer. This nanocomposite sample was then injected directly into the SANS cell, which was cleaned and assembled beforehand. Some of the samples were then taken directly to the beam line for measurements and put in the sample holder at 37°C. For samples that were not measured immediately, they were placed in an oven at 37°C for four hours to cure. Since the samples were measured in SANS right after synthesis, kinetic measurements could be taken for some of the samples to investigate the gelation process.

2.5 Vibrating Sample Magnetometer

The vibrating sample magnetometer (VSM) can measure the magnetic moment of a material as a function of magnetic field, temperature, angle and time. In these studies, magnetic hysteresis loops of the samples were measured. A sample is placed in a uniform magnetic field between two inductive coils and is vibrated sinusoidally. An electric current that is proportional to the saturation magnetization is produced in the coils. From this information, a hysteresis curve can be obtained[25,26]. A hysteresis loop measures the magnetic moment of a sample as an alternating magnetic field is applied. Magnetic materials require a magnetic field in the opposite direction to become demagnetized. The hysteresis loop traces this path from magnetization to demagnetization. Saturation magnetization refers to the magnetic moment at which all the dipoles in the sample are in alignment with the magnetizing field direction. Coercivity can also be measured and describes the magnetization required to reduce the magnetization to zero after a sample has reached saturation. The VSM samples were prepared at the same time as the SANS samples and placed directly into VSM sample screw top capsules. They were cured for two hours at 37°C after vortex mixing and then stored in a refrigerator until use. VSM measurements were made at the University of Maryland, College Park.

Chapter 3

Structural Characterization of Nanoparticles

3.1 Introduction

Structural properties of the iron oxide nanoparticles can be examined using TEM characterization techniques. The behavior of the magnetite nanoparticles prior to embedding in the SELP polymer needs to be examined. By characterizing the nanoparticles in water solution, preliminary information about the nanoparticles can be obtained. This data can later be used for comparison with data gathered after the nanoparticles are introduced to SELP. This comparison will help in understanding the effect that the polymer structure from SELP has on ordering of the nanoparticles.

3.2 TEM Analysis

Transmission electron microscopy (TEM) was used to investigate nanoparticle samples. The focus of the analysis is primarily on comparing the effects of nanoparticle behavior with different coatings and sizes of nanoparticles. We examined 50 nm hydrodynamic diameter nanoparticles that are coated with a single dextran layer, or a double layer that is functionalized with amine or maleimide, and compared the nanoparticle behavior between surface coatings. The same was done for different nanoparticle diameters, 30, 50 and 80 nm. It was found that each distinct surface coating and size affected the behavior of the nanoparticles.

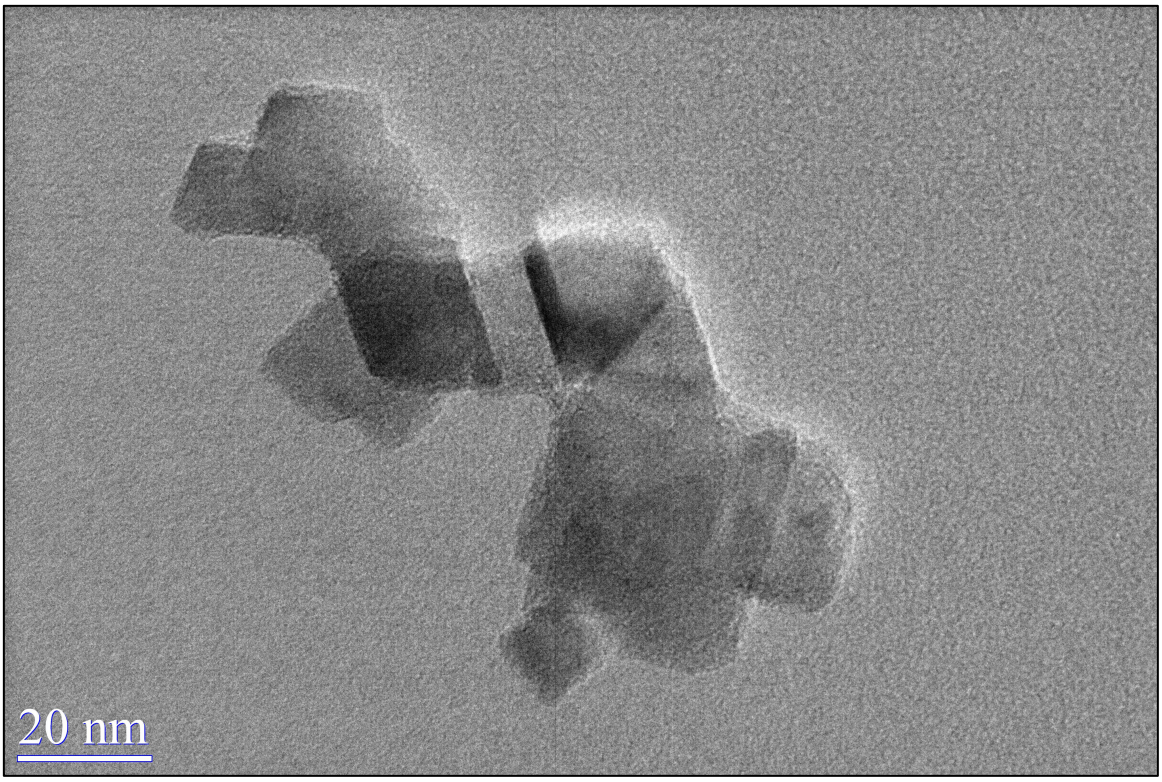

Figure 3.1 TEM of 50 nm nanoparticles with single dextran coat, air-dried on TEM grid

Figure 3.1 is a TEM image of a 50 nm particle with a single dextran layer. Immediately noticeable is the clustering of several nanoparticles and also the square shape of each of the particles. It is also apparent that the size of the nanoparticles observed here is much less than the DLS diameter of 50 nm, they are closer to 20 nm in diameter. Clustering of the nanoparticles is expected due to drying effects, however it is believed that the dextran coat reduces aggregation only in solution. There is also a significant particle size range that is observed in the cluster in figure 3.1. The smallest particle is about 10 nm, while the largest particle diameter is closer to 30 nm. Most particles tend to be in the 20 nm diameter range. The sizes measured by TEM are smaller than the DLS measured nanoparticle size of 50 nm. This was expected as DLS gives a hydrodynamic size of the nanoparticles in solution. When the dextran coat is in solution, it expands outwards, thus

increasing the size measured by DLS. Since the TEM samples are dry, their overall diameter would be expected to be smaller. The overall cluster size of this sample seems to be similar to other samples at this size with different surface coatings. There is no evidence of strong chaining with these nanoparticles, although the cluster has a slightly linear structure. Many of the nanoparticles tend to overlap with one another, making single particle identification difficult. The clustering seen in figure 3.1 is a couple of nanoparticles wide, which can be attributed to the sample preparation technique required for these samples. Since the nanoparticle solutions are dropped on a TEM grid and then air-dried, this method of drying could cause the nanoparticles to cluster, which is what is seen in the resulting microscopy images. The dextran layer seems to have a minimal effect on restricting clustering, as the nanoparticles are overlapping one another and do not seem to be dispersed at all.

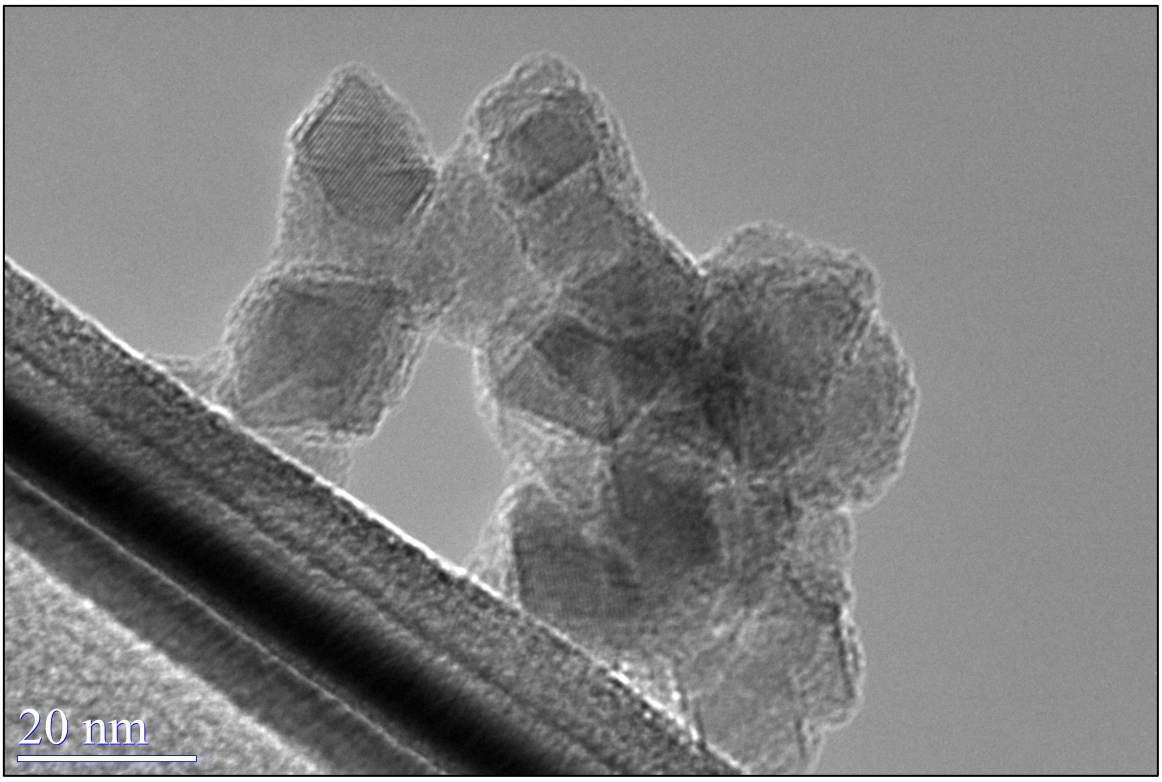

Figure 3.2 TEM of 50 nm nanoparticles with amine coat, air-dried on TEM grid

With the addition of an amine functionalization to the single dextran layer, we can examine the nanoparticles as seen in figure 3.2. The size range of these nanoparticles seem to be slightly narrower, with the smallest particles being about 15 nm in diameter and the largest around 20 nm. Again, as seen from the previous sample, the diameter is smaller than the DLS measured size, which is expected. The size of the entire amine coated nanoparticle cluster is about 50 nm in diameter, only a few nanoparticles wide, slightly larger than the cluster of single dextran coated nanoparticles seen in figure 3.1. Evidence of chaining is not present for the amine coated nanoparticles. The identification of a single particle for size measurements is difficult due to the aggregate nature and overlapping of many of the nanoparticles in the image. However, the unidirectional crystallographic grains observed can identify several single particles in figure 3.2.

The final coating to be examined is the 50 nm nanoparticles with a maleimide coating. This sample is imaged below in figure 3.3.

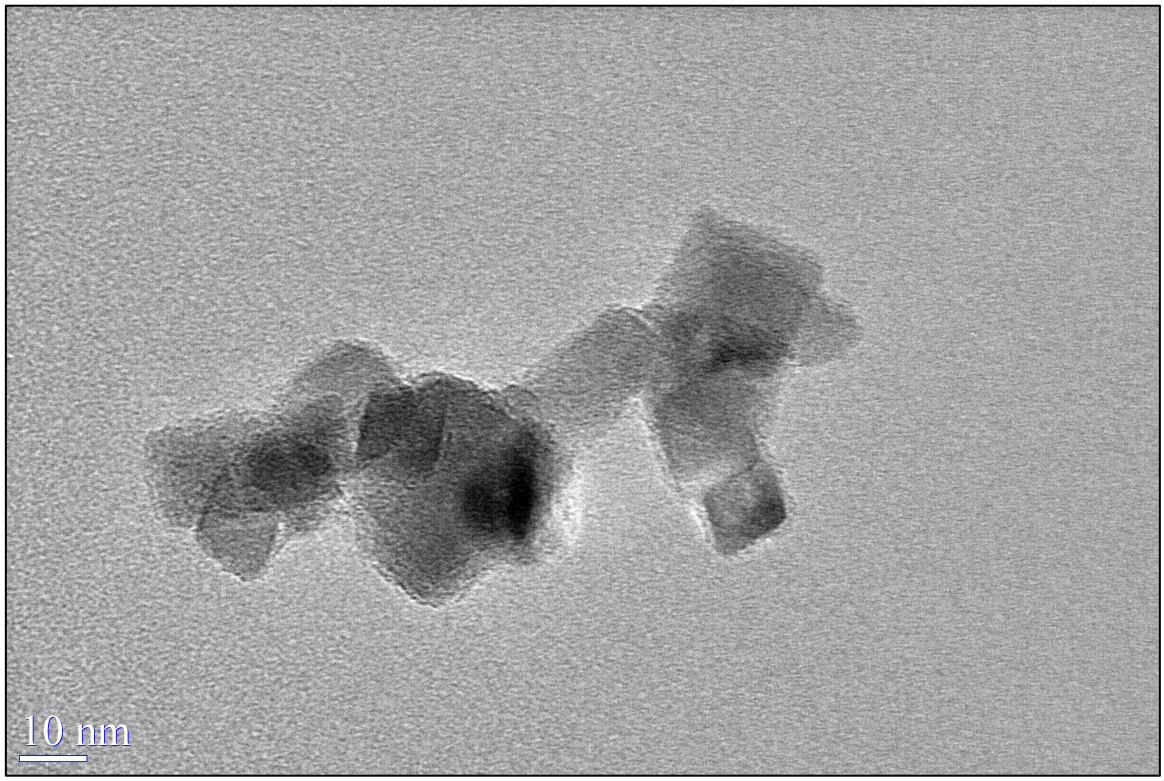

Figure 3.3 TEM of 50 nm nanoparticles with maleimide coat, air-dried on TEM grid

These maleimide coated nanoparticles particles tend to be smaller, with many being around 10 nm in diameter and the largest about 25 nm. These larger nanoparticles follow the same size range seen in the single dextran and amine coated nanoparticles. The darker areas in the image indicate overlapping nanoparticles, which is evident in this sample. Linear, single particle chaining structure is minimal, however multiple nanoparticles seem to form short linear segments. These segments could be indicative of nanoparticle chaining. The addition of maleimide does not seem to increase dispersion or prohibit clustering in the sample. The crystallinity of several of the nanoparticles can be observed. In figure 3.4 below, a single maleimide coated nanoparticle is imaged at high resolution.

The lattice fringes and crystallographic direction of these fringes can be observed. From the TEM image, each nanoparticle looks to have a singular crystallographic grain direction, which could help identify individual nanoparticles among clusters.

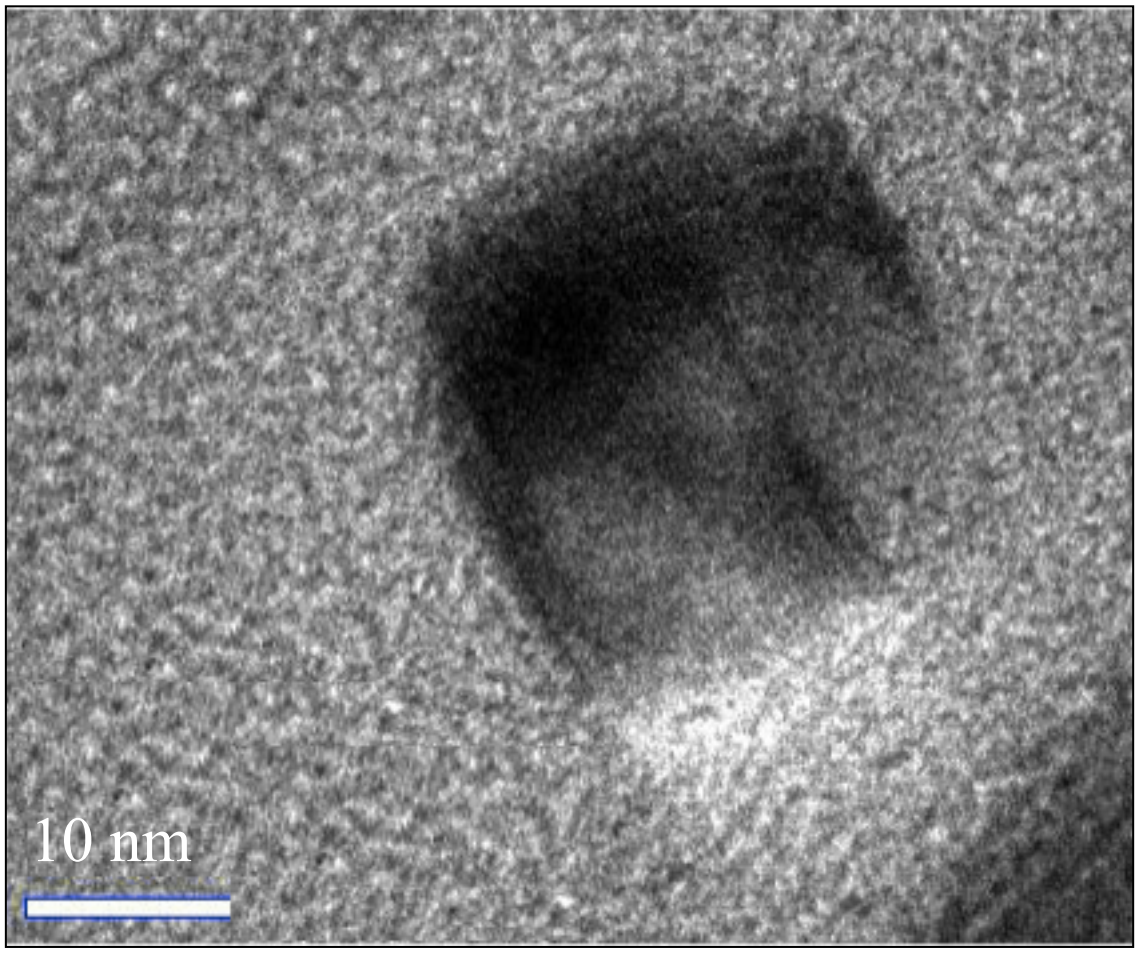

Figure 3.4 TEM of single 50 nm nanoparticle with maleimide coat at high resolution

The iron oxide core is easily visible, however the surrounding dextran coating is not. These nanoparticles have the same square shape as seen in the single dextran layer nanoparticle sample (figure 3.1) and a single crystallographic grain direction is observed. Between the three different types of coatings, none seem to prohibit clustering more than the other coatings. The TEM images of the three different coated nanoparticle samples

are not the same as size measurements made in the DLS, most likely due to the difference between a wet hydrodynamic size and a dry size. The crystallinity of the nanoparticles was observed most clearly in the amine coated nanoparticle, with crystal grains running unidirectional for each nanoparticle. Clustering is found to be dominant, especially in the amine coated nanoparticle sample. Any chaining that was observed by the nanoparticles clustered into wide chain segments that were a few nanoparticles thick and had heavy overlapping of particles.

3.4 VSM Analysis

The magnetometry of the nanoparticles was previously measured at room temperature using a MPMS SQUID magnetometer from Quantum Design by Christine Lau. The resulting hysteresis loop can be seen below in figure 3.5.

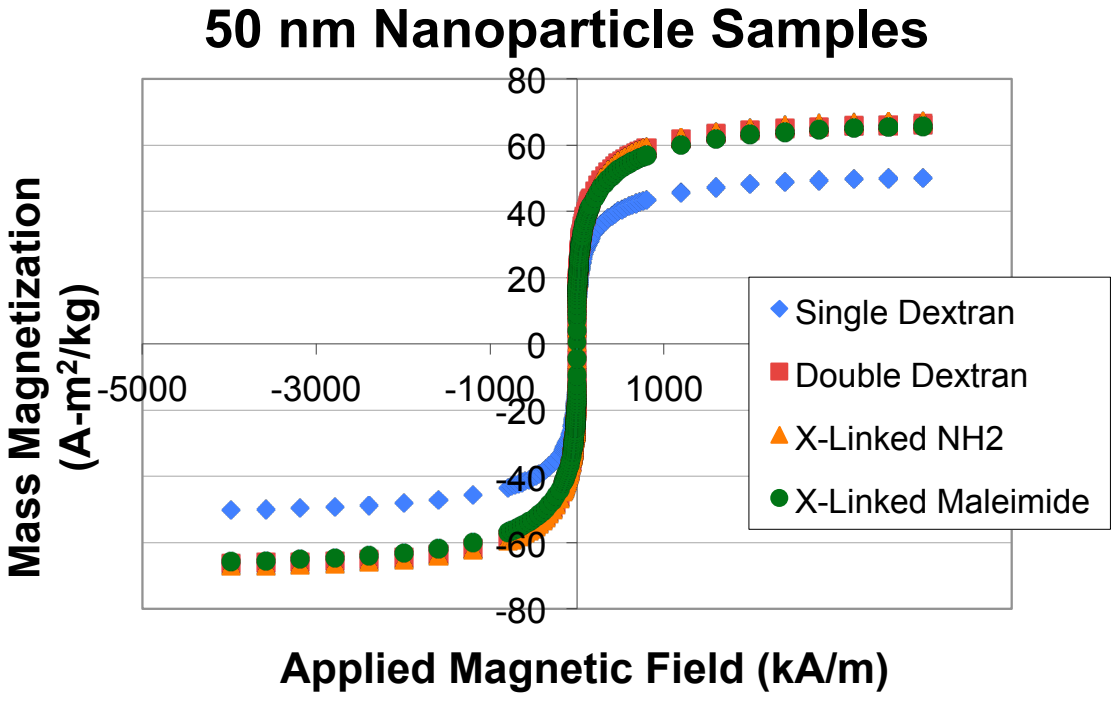

Figure 3.5. Magnetic hysteresis loop at room temperature of 50 nm nanoparticles in water

The saturation magnetization of the nanoparticles is found to be between 50-66 Am^2/kg. Single dextran exhibits the smallest saturation magnetization of 50 Am^2/kg, while the other coatings have similar saturation values of around 66 Am^2/kg. A reduction of the saturation magnetism is expected when compared to bulk magnetite due to the presence of the dextran shell, which contains diamagnetic properties. However, it is not clear why single dextran exhibits the smallest saturation between the different functionalities. For hyperthermia therapy, saturation magnetization believed to be the most important magnetic property of the nanoparticles[27]. It affects the length of time and dosage of hyperthermia treatments. There is no coercivity measured in the hysteresis loop for any of 50 nm nanoparticles. However, due to the presence of interactions, this system is not superparamagnetic. This measurement can be compared to magnetometry measurements after the addition of the SELP with the nanoparticles.

Chapter 4

Magnetometry of Nanoparticles and SELP System

4.1 Introduction

Hysteresis measurements of the nanoparticles and SELP nanocomposite system were taken using a vibrating sample magnetometer (VSM). The magnetic field (Tesla) versus magnetic moment, μ (J/T) was plotted and then fitted to a Langevin function using Origin 8.1. The Langevin equation for paramagnetism is as follows[1]:

$$M(H) = N\mu \left[\coth(x) - \left(\frac{1}{x}\right)\right]$$

$$x = \frac{\mu H}{k_B T}$$

where:

M = magnetization [T]
H = field [T]
N = number of particles
μ = magnetic moment [J/T]
k_B = Boltzmann's constant [1.38x10^{-23} J/K]
T = temperature [298 K]

From the fitting parameters, the magnetic moment of the nanoparticles and the approximate number of nanoparticles can be calculated. The saturation magnetization, which is believed to be the most important factor for hyperthermia applications, is calculated by multiplying the number of particles by the magnetic moment and dividing by the mass[28]. The Langevin equation for paramagnetism is an approximate fit. Paramagnetic materials have no coercivity, however several of the nanocomposite samples exhibited small coercivity values and were fitted with the Langevin equation.

These samples demonstrate ferromagnetism by containing some coercivity[1]. Each sample is normalized by nanoparticle mass for direct comparison with one another.

4.2 Magnetic Hysteresis Measurements

The magnetometry of the samples were examined through VSM measurements. The saturation magnetization and virgin magnetization curves (the hysteresis before a magnetic material reaches saturation) of each sample were determined. In figure 4.1 below, the hysteresis loop for the 80 nm, single dextran coated nanoparticles with 4 wt.% SELP sample is shown.

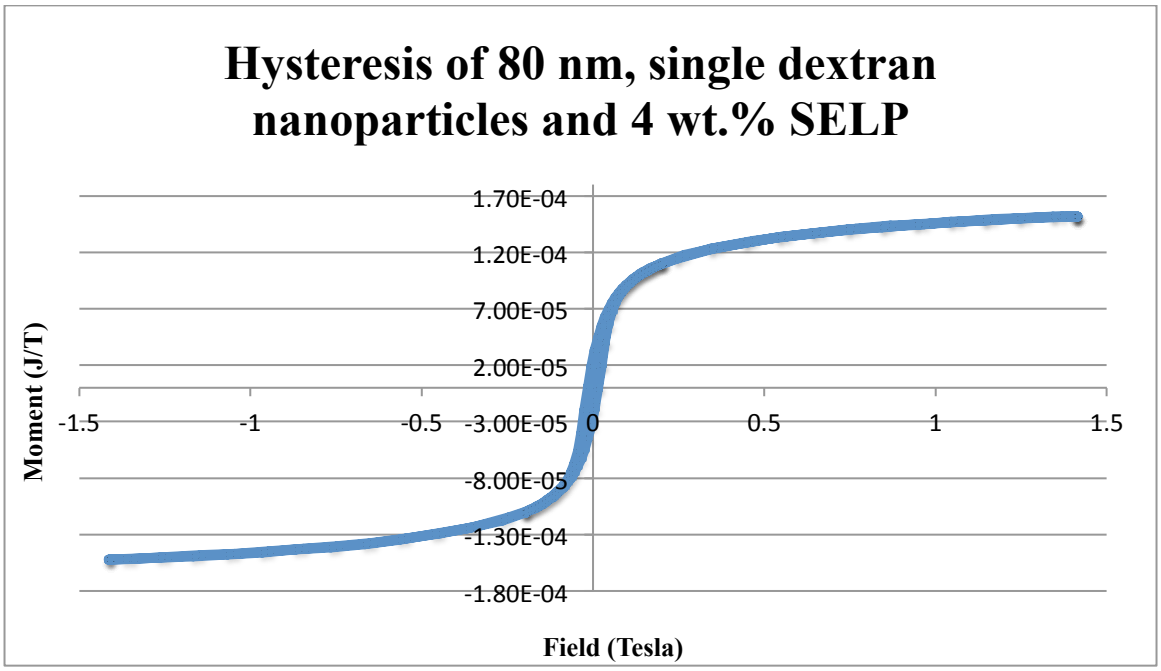

Figure 4.1 Magnetometry of 80 nm, single dextran nanoparticles and 4 wt.% SELP

The saturation magnetization is found to be approximately 36 Am^2/kg after mass normalization. This value for saturation magnetization is similar to other samples, with saturation magnetization values typically varying between 20-51 Am^2/kg. All of the saturation magnetization values for the nanocomposite system, with the exception of two

samples, are smaller than the saturation magnetization values found for just the nanoparticles. The presence of SELP likely adds diamagnetic influence, thus lowering the saturation magnetization of the nanocomposite samples. A small amount of coercivity also exists in the sample. In paramagnetic samples, the hysteresis loop, including the virgin curve, would be a single line that goes through the origin. However, there is a small amount of resistance from the sample to being demagnetized. This means the sample is ferromagnetic and that the nanoparticle and SELP nanocomposite systems have changed the properties[29]. Figure 4.2 below offers an expanded view at the coercivity found in the sample.

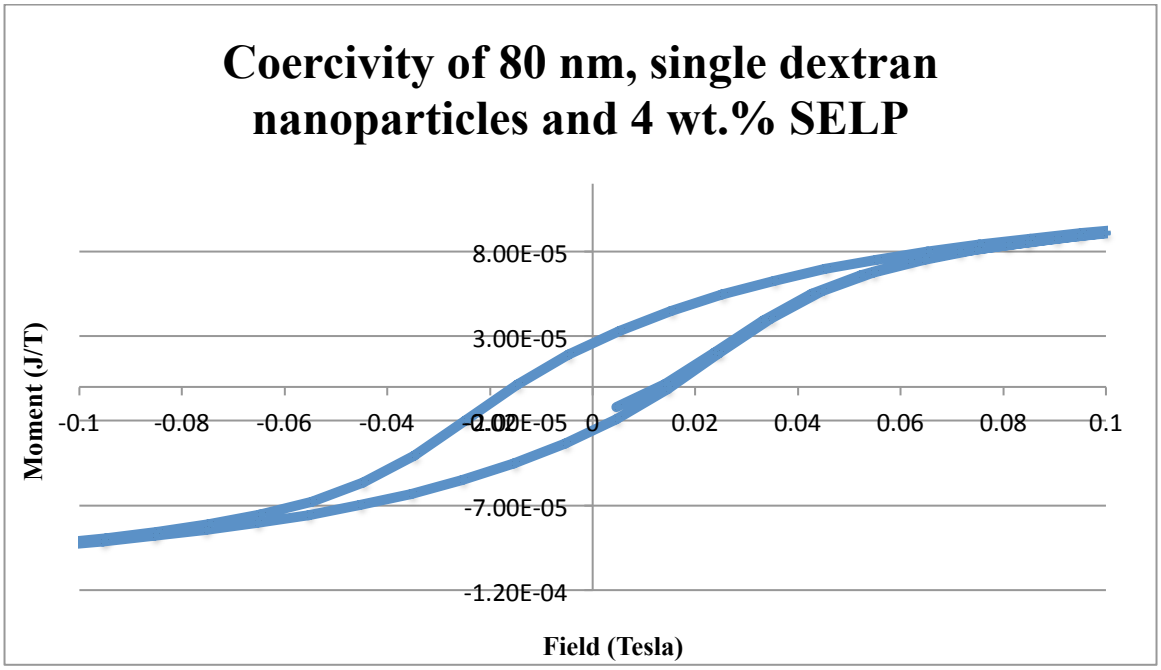

Figure 4.2 Expanded view of coercivity observed in the 80 nm, single dextran nanoparticles and 4 wt.% SELP sample

The coercivity signal achieved is extremely small, about 15.3 mT, but the presence of a small coercivity is interesting and unexpected for these samples. All of the samples with SELP demonstrated some coercivity. The largest nanoparticle size, 80 nm in diameter,

gave the greatest coercivity values (13-17 mT), while the smallest nanoparticle size, 30 nm in diameter, exhibited the smallest coercivity values (5-6 mT). Despite the presence of a small amount of coercivity, these samples will be fit to the Langevin equation for paramagnetism as an approximation.

4.3 Langevin Fitting

The Langevin equation for paramagnetism is applied to the hysteresis curves of each sample. The values for constants, c1 and c2, can be used to calculate N, the number of nanoparticles and μ, the magnetic moment of the sample. c1 represents N times μ, and c2 is the magnetic moment, μ, divided by Boltzmann's constant, k_B, and temperature, T. μ can be calculated first, since k_B and T are known values and c2 is given by the Langevin fit. Once μ is calculated, c1 can be divided by μ to find N. Below is an example of a Langevin fit and the resulting c1 and c2 parameters. The hysteresis loop of the 80 nm, single dextran nanoparticles with 4% SELP sample is seen in figure 4.3. The Langevin fit values are seen in the table, with the fit plot seen on the graph as a red line.

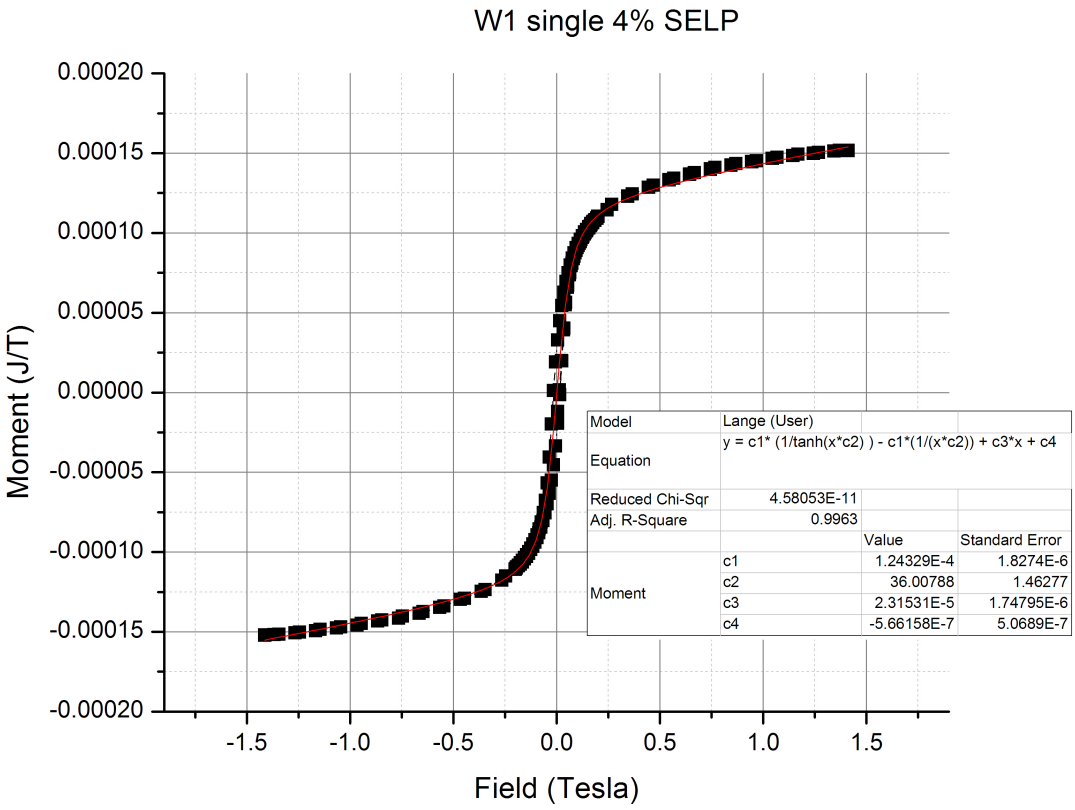

Figure 4.3 Langevin fit and hysteresis loop of 80 nm, single dextran nanoparticles and 4 wt.% SELP

The Langevin equation fits this sample relatively well. However, the fit of the data approaching saturation magnetization is not completely represented by the Langevin equation. The samples tend to reach saturation at a faster rate than what the Langevin equation is able to model. Also, there is a small amount of coercivity seen in the sample. The Langevin equation goes through the origin and does not account for any coercivity, which is typically present in ferromagnetic materials. Besides these slight discrepancies, the Langevin equation fits all of the samples relatively well. The Langevin equation also provides important information from the fitting parameters. The number of particles, N, and the magnet moment, μ, for each sample was calculated from the Langevin fits and these values are listed below in table 4.1. Each sample was measured once and the

standard deviation of these values was calculated from the fitting. The mass saturation magnetizations of the samples are calculated by dividing the saturation magnetization by the mass of each nanoparticle for normalization. The mass of the nanoparticle concentration is found from multiplying the volume of the nanoparticles in the sample by the concentration of the nanoparticles. Coercivity is measured directly from the hysteresis data of each sample by examining the magnetization field value where the hysteresis loop crosses the x-axis. Standard deviation is calculated by examining the offset of the magnetometer used. Values for mass saturation magnetization and coercivity for each sample are also listed in table 4.1 below.

Samples	*Number of Nanoparticles*	*μ [Bohr Magneton]*	*Saturation Magnetization [Am^2/kg]*	*Coercivity [mT]*
80 nm single 4% SELP	$8.40 \times 10^{14} \pm 1.8 \times 10^{14}$	$1.60 \times 10^{4} \pm 3.6 \times 10^{2}$	36 ± 6.2	15.3 ± 3.3
80 nm single redo 4% SELP	$2.56 \times 10^{15} \pm 1.8 \times 10^{14}$	$1.49 \times 10^{4} \pm 3.6 \times 10^{2}$	51 ± 6.2	15.5 ± 3.3
80 nm double 8% SELP	$1.89 \times 10^{15} \pm 1.8 \times 10^{14}$	$1.52 \times 10^{4} \pm 3.6 \times 10^{2}$	85 ± 6.2	16.5 ± 3.3
80 nm NH2 4% SELP	$2.08 \times 10^{15} \pm 1.8 \times 10^{14}$	$1.72 \times 10^{4} \pm 3.6 \times 10^{2}$	49 ± 6.2	14.2 ± 3.3
80 nm NH2 8% SELP	$4.85 \times 10^{14} \pm 1.8 \times 10^{14}$	$1.61 \times 10^{4} \pm 3.6 \times 10^{2}$	20 ± 6.2	12.9 ± 3.3
80 nm Mal 4% SELP	$9.34 \times 10^{14} \pm 1.8 \times 10^{14}$	$1.52 \times 10^{4} \pm 3.6 \times 10^{2}$	20 ± 6.2	14.3 ± 3.3
50 nm single 4% SELP	$9.20 \times 10^{14} \pm 1.8 \times 10^{14}$	$1.59 \times 10^{4} \pm 3.6 \times 10^{2}$	30 ± 6.2	9.6 ± 3.3
50 nm single 9x dilution 4% SELP	$7.07 \times 10^{13} \pm 1.8 \times 10^{14}$	$1.74 \times 10^{4} \pm 3.6 \times 10^{2}$	27 ± 6.2	10.8 ± 3.3
50 nm double 4% SELP	$7.49 \times 10^{14} \pm 1.8 \times 10^{14}$	$1.71 \times 10^{4} \pm 3.6 \times 10^{2}$	42 ± 6.2	9.9 ± 3.3
50 nm double 8% SELP	$6.25 \times 10^{14} \pm 1.8 \times 10^{14}$	$1.60 \times 10^{4} \pm 3.6 \times 10^{2}$	32 ± 6.2	9.7 ± 3.3
50 nm NH2 4% SELP	$1.07 \times 10^{15} \pm 1.8 \times 10^{14}$	$1.42 \times 10^{4} \pm 3.6 \times 10^{2}$	23 ± 6.2	9.4 ± 3.3
50 nm NH2 8% SELP	$5.35 \times 10^{14} \pm 1.8 \times 10^{14}$	$1.76 \times 10^{4} \pm 3.6 \times 10^{2}$	44 ± 6.2	8.6 ± 3.3
50 nm Mal 4% SELP	$9.69 \times 10^{14} \pm 1.8 \times 10^{14}$	$1.62 \times 10^{4} \pm 3.6 \times 10^{2}$	32 ± 6.2	9.7 ± 3.3
50 nm Mal 8% SELP	$1.75 \times 10^{14} \pm 1.8 \times 10^{14}$	$1.57 \times 10^{4} \pm 3.6 \times 10^{2}$	113 ± 6.2	9.6 ± 3.3
30 nm single 4% SELP	$7.35 \times 10^{13} \pm 1.8 \times 10^{14}$	$2.00 \times 10^{4} \pm 3.6 \times 10^{2}$	32 ± 6.2	5.1 ± 3.3
30 nm double 8% SELP	$2.88 \times 10^{14} \pm 1.8 \times 10^{14}$	$1.44 \times 10^{4} \pm 3.6 \times 10^{2}$	27 ± 6.2	5.9 ± 3.3

Table 4.1 Table of the number of nanoparticles (N), the magnetic moment (μ), saturation magnetization and coercivity found through Langevin fitting.

Calculated from the Langevin fit, the number of nanoparticles, N, is in the range of 10^{13} to 10^{15} nanoparticles per sample range. The magnetic dipole moment of the samples is presented in terms of Bohr magnetons. Given the number of atoms expected in a sample and the fact that there are two Bohr magnetons per atom, these values are reasonable[29]. The saturation magnetization of the nanocomposite samples is smaller than the 50-66 Am^2/kg saturation magnetization found for the nanoparticle only sample. A lower saturation field is ideal for the applications of the nanocomposite system for cancer metastases over a large area of the body. However, this also limits the field range in which the nanocomposite system will have effective heat generation from hysteresis loss. The coercivities have an error based on the offset of the VSM used. It was found that the nanoparticles exhibit a non-negligible coercivity, although small. Nanoparticles without SELP did not demonstrate any coercivity, as seen in figure 3.5. This indicates that the addition of SELP encourages anisotropy in the sample. The coercivities are found to be dependent on nanoparticle size, with the 80 nm nanoparticle samples giving the largest coercivities values and the 30 nm nanoparticle samples giving the smallest coercivities. This suggests that there is a size dependence based on the stabilized clustering of the nanoparticles in the sample due to the presence of SELP.

4.4 Nanoparticle Concentrations

After normalization by mass, the samples can be directly compared to one another. The hysteresis of similar samples are plotted together and ideally the curves should be identical because they will have the same nanoparticle concentrations. However, this was not found to always be the case. In figure 4.4 below, both of the 50 nm, single dextran coated nanoparticles with 4 wt.% SELP samples are plotted. These samples should be

identical to one another since they were synthesized with identical procedures and nanoparticle and SELP chemistry. However, there are subtle differences between the hysteresis loops of the sample.

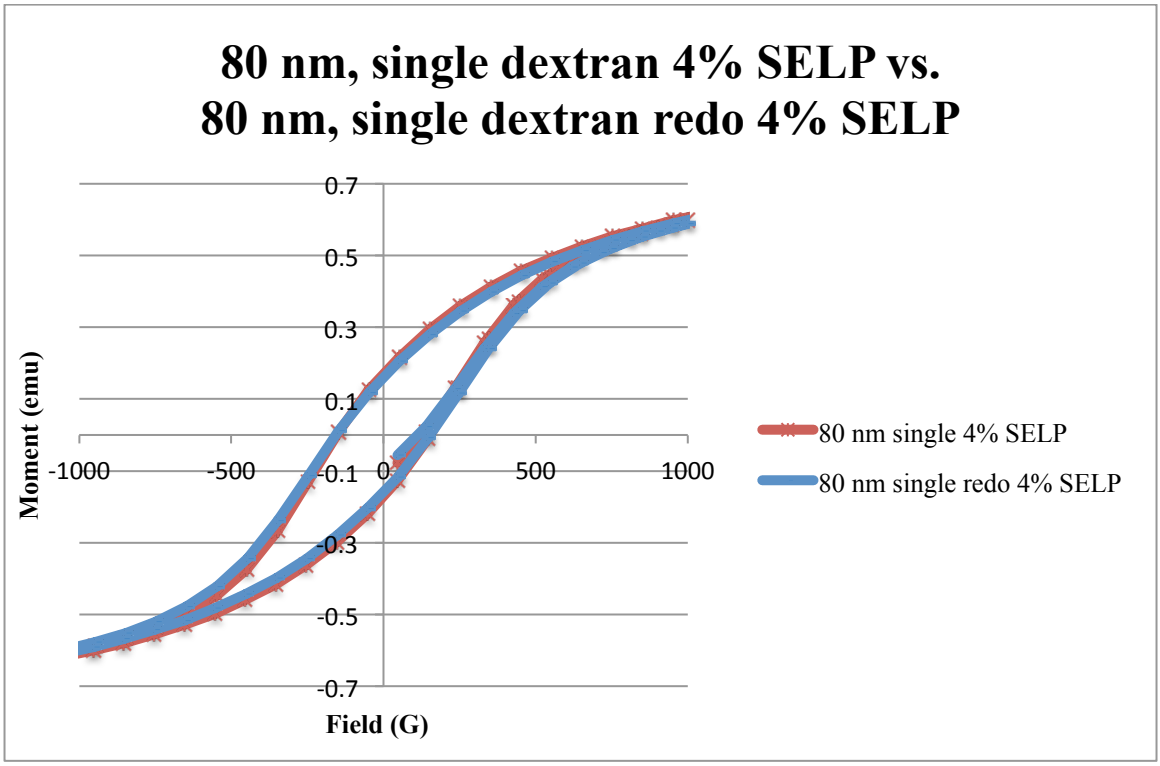

Figure 4.4 Hysteresis plot of both 80 nm, single dextran nanoparticles with 4 wt.% SELP samples, original and the redo

As the magnetization approaches saturation, the curves of the samples differ slightly. The original sample in red appears to approach saturation just a bit more quickly than the redo sample. The nanoparticle concentration between these samples should be the same, however they are different as seen from the different hysteresis loops. Because there exists a slight difference between the two curves, the nanoparticle concentrations are not quite what is expected. This same variation is more obvious between the 50 nm, single

dextran coated nanoparticles and 4 wt.% SELP, original solution and 1/9 diluted nanoparticle concentration. Both hysteresis loops for the 50 nm, single dextran coated and 4 wt.% SELP samples are plotted below in figure 4.5.

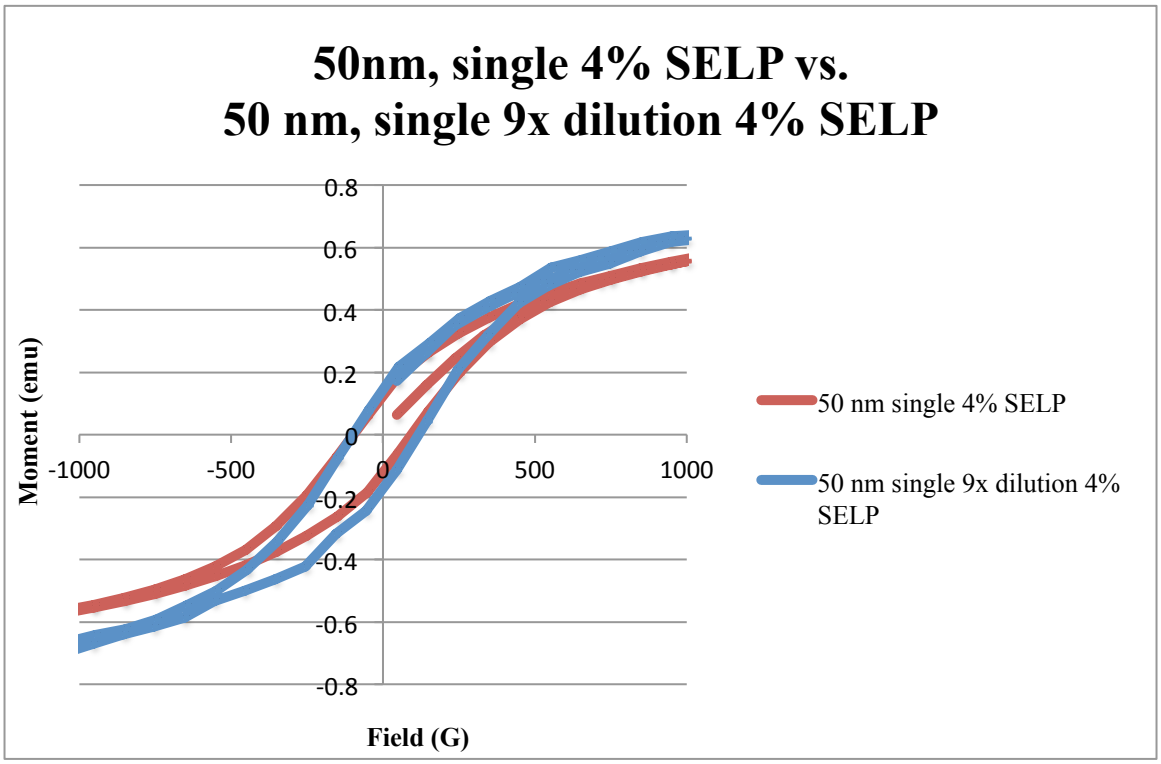

Figure 4.5 Hysteresis plot of both 50 nm, single dextran nanoparticles with 4 wt.% SELP samples, original solution and 1/9 dilution

After mass normalization, the hysteresis loops between these two samples should be identical, as the nanoparticles in both samples are the same. However, just like the 80 nm, single dextran nanoparticles and 4 wt.% SELP samples seen in figure 4.4, they were not identical. Figure 4.5 demonstrates the variance between the two 50 nm, single dextran nanoparticles with 4 wt.% SELP samples. Again, the samples approach saturation at different rates, as well as have slightly different coercivities. The synthesis process could be to blame for this slight variation. This indicates that sample reproducibility is not

always reliably guaranteed. This difference between samples of the same nanoparticles is only consistently seen in the single dextran coated nanoparticle samples. This was not the case for nanoparticles with double dextran, amine and maleimide coatings. In figure 4.6, 50 nm double dextran nanoparticles with 4 wt.% and 8 wt.% SELP are plotted together.

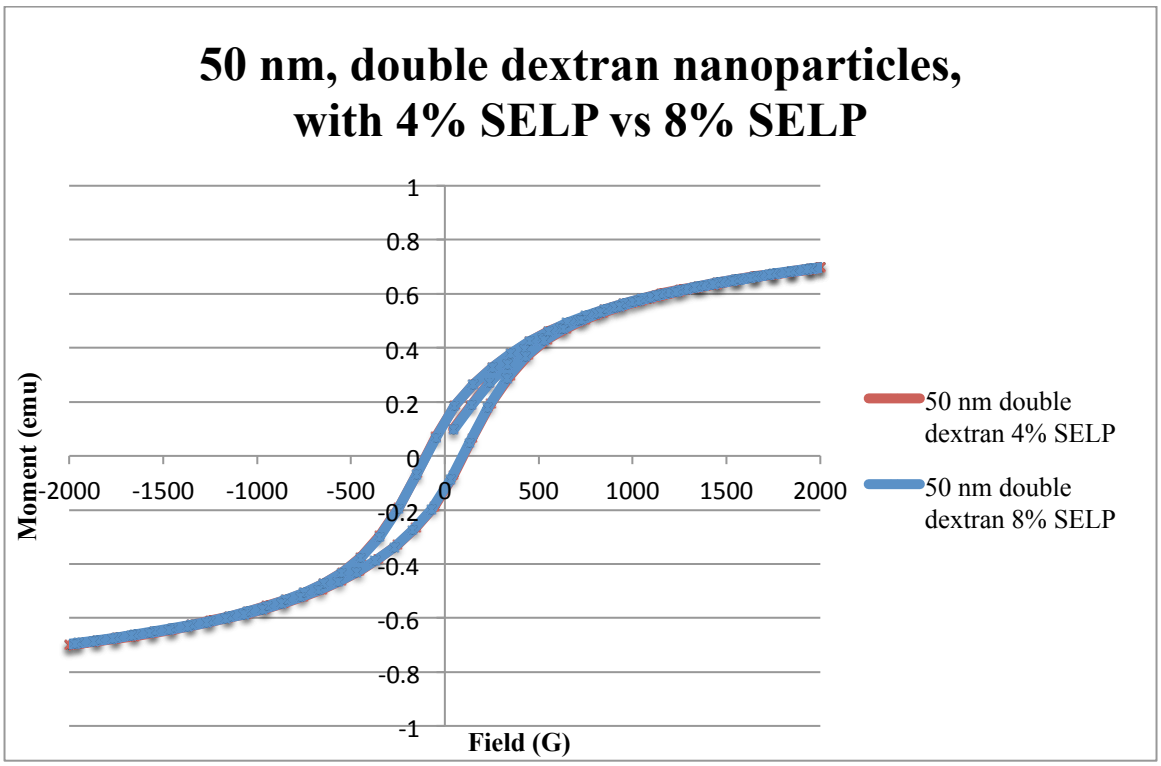

Figure 4.6 Hysteresis plots of 50 nm, double dextran nanoparticles with 4 wt.% and 8 wt.% SELP samples

After these graphs are normalized by mass, they should have identical hysteresis curves. The double dextran coated nanoparticles follow this, while it was observed earlier that the single dextran coated nanoparticles did not. Similarly to the double dextran coated nanoparticles, the other functionalized nanoparticles with amine and maleimide coatings also have consistent nanoparticle concentrations between 4 wt.% and 8 wt.% SELP samples. Only the single dextran coated nanoparticle and SELP nanocomposite samples showed variation between samples after normalization. The single dextran coated

nanoparticles will exhibit the greatest interactions with one another, while the double dextran, amine and maleimide coated nanoparticles have weaker particle interactions.

Chapter 5

TEM of Nanoparticles and SELP System

5.1 Coating Comparison

Transmission electron microscopy of the nanoparticle and SELP nanocomposite system was performed to compare different coatings on the particles and how they affect structural interactions with SELP. The coating series that is being compared below is a 50 nm particle with coatings of a single layer of physically adsorbed dextran, or a double layer functionalized with amine and maleimide. Amine is negatively charged and maleimide is positively charged, creating steric effects between interacting nanoparticles. The steric repulsion present is important to minimize aggregates.

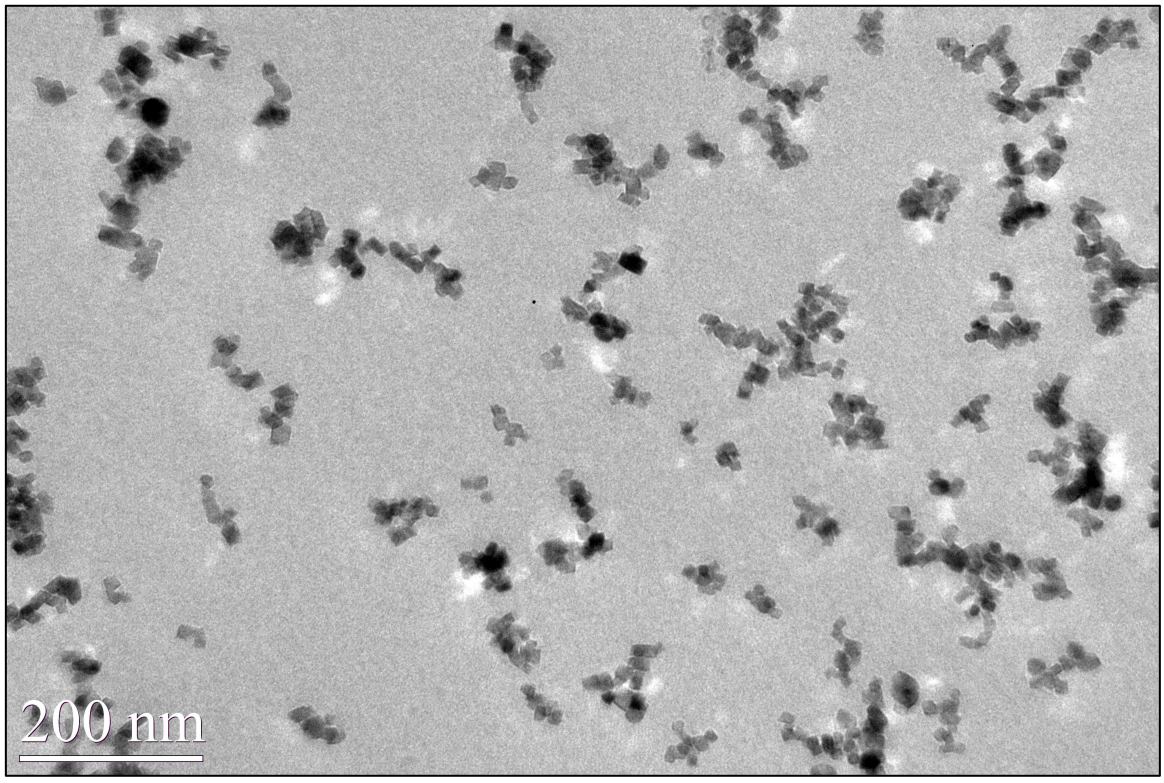

Figure 5.1 TEM of 50 nm nanoparticles with single dextran coating and 4 wt.% SELP embedded in resin

Above, in figure 5.1, is a 50 nm particle with a single dextran coating in 4 wt.% SELP embedded in resin. Chaining of the nanoparticles is evident in the microscopy image. Small clumps of nanoparticles are still apparent, however chaining is dominant. Nanoparticles mostly follow a linear pattern with branching chains of nanoparticles occurring. On average, a single nanoparticle is around 20 nm wide. Chaining as long as 300 nm can be seen in the top right corner of Figure 5.1. Clusters of only two or three nanoparticles long are also observed. The clusters of nanoparticles tend to align linearly, even though they still form small aggregates. The nanoparticle chains also exhibit some branched sections, which could represent the cross-link points of SELP polymer. The nanoparticles tend to align a couple of nanoparticles wide, instead of single width nanoparticle chaining. The single layer of dextran optimizes steric interactions between the nanoparticles and reduces aggregation. The dextran coating between nanoparticles limits how close the nanoparticles can approach causing them to remain slightly separate from one another without resulting in large aggregates. There are two possibilities for nanoparticle-SELP interactions. First, the nanoparticle chains could possibly be templating the SELP network and aligning along a polymer matrix. The nanoparticle chains do not cover an entire length of SELP network fiber. The nanoparticles seem to be dispersed throughout the SELP network, templating only portions of the structure. Another option is that the nanoparticles are aggregating into the pores of the SELP network. The nanoparticles that are observed in figure 5.1 could indicate the spacing in between the polymer mesh. Both possible structures are illustrated below. In figure 5.2, a schematic of the nanoparticles templating SELP network structure is drawn in blue over the original TEM image.

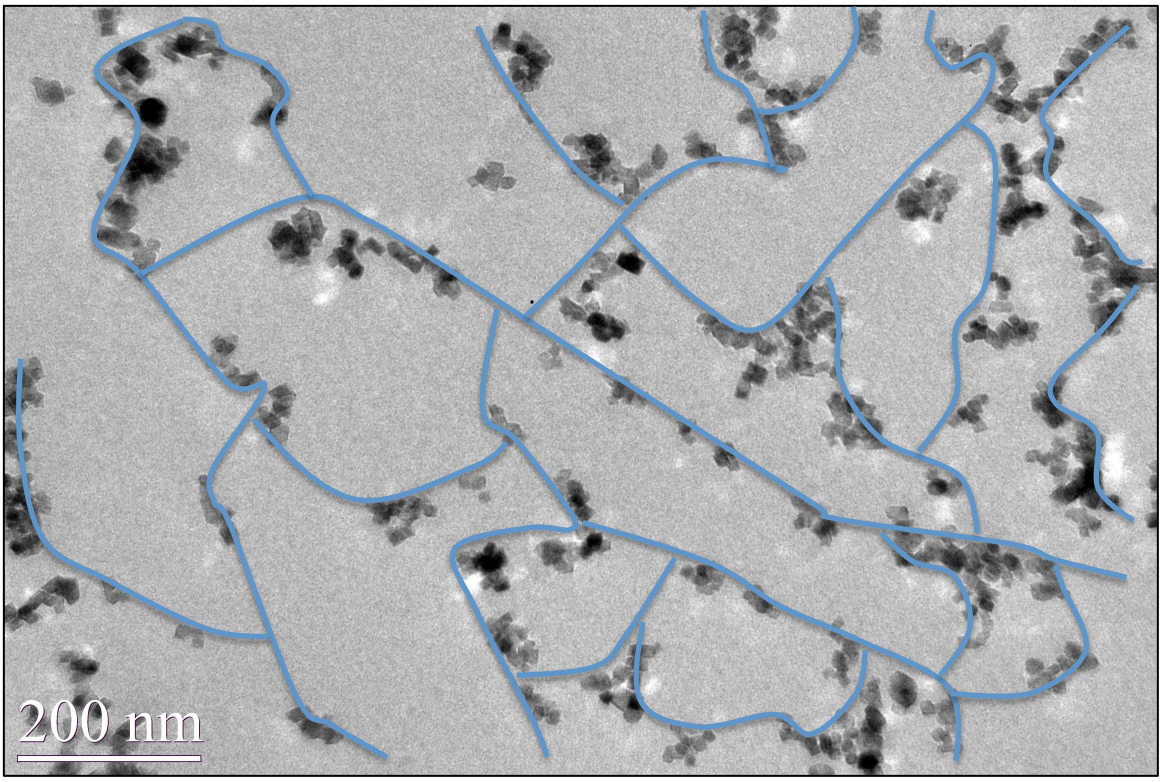

Figure 5.2 TEM of 50 nm nanoparticles with single dextran coating and 4 wt.% SELP TEM image with schematic of templating SELP network outlined in blue

This is a rough schematic of the SELP network structure, but if the nanoparticles are templating the structure of the SELP, then this basic outline could be possible. The nanoparticles are chaining according to where the polymer matrix is. The position of the nanoparticle chains lightly outlines the polymer network in the above image. A denser polymer network may exist, but if it is not completely templated with nanoparticles then it is difficult to image with certainty. This option seems likely, as the nanoparticles interact with the SELP matrix and are encouraged to chain with the SELP structure, which also confirms VSM findings of increased coercivity with the presence of SELP. A second option exists, as seen in figure 5.3 below. This schematic demonstrates the possibility that the nanoparticles are positioned in the open space between polymer strands. The polymer network only exists around the nanoparticle chains and clusters.

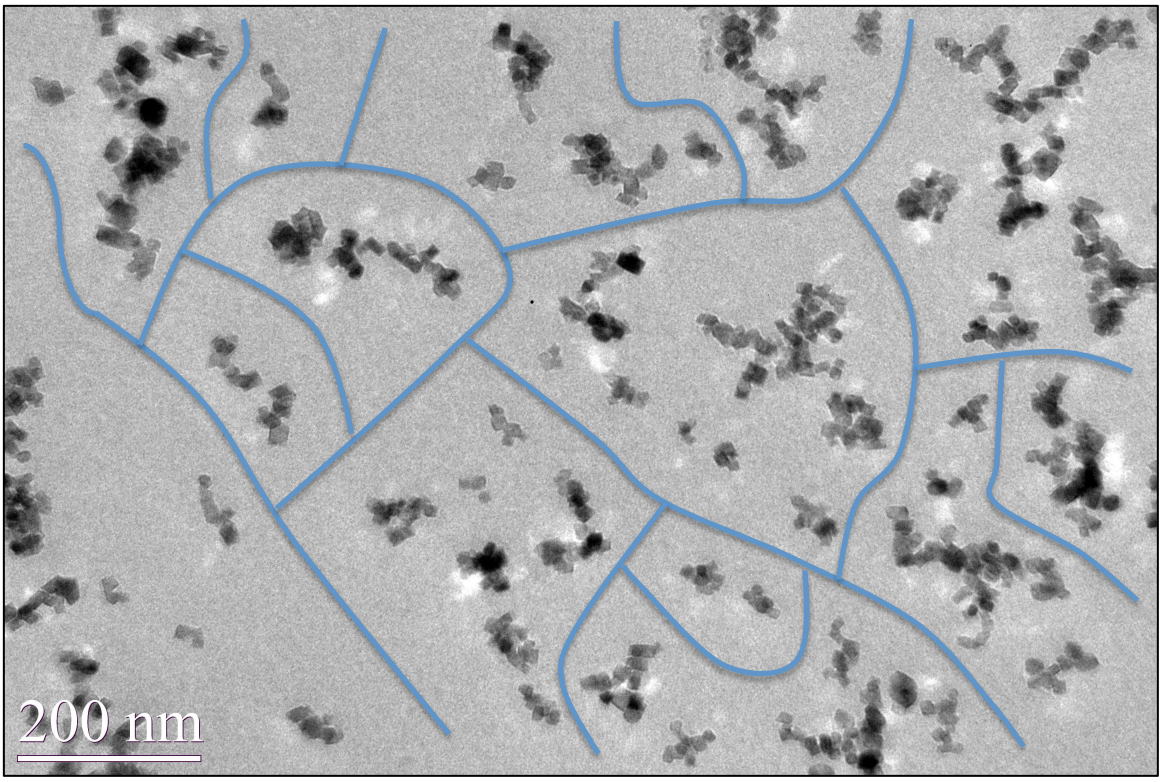

Figure 5.3 TEM of 50 nm nanoparticles with single dextran coating and 4 wt.% SELP TEM image with schematic of the intermediate SELP network outlined in blue

A different SELP network emerges when the polymer network is envisioned intermediate to the nanoparticles. The SELP network could be dictating the chaining of the nanoparticles or the nanoparticles could be chaining without any influence from the SELP and residing between polymer chains because there is space. This model seems less likely, as the nanoparticles would need to chain on their own without any influence from SELP. If this was the case, then nanoparticle chaining would have been observed in the TEM images of the nanoparticle only samples. Since the SELP is very difficult to image in the TEM, it is difficult to know if the nanoparticles are templating the SELP or fitting within the polymer pores. The nanoparticles do exhibit chaining with the addition of the SELP system, which indicates that the inclusion of SELP promotes organization/texture within the nanoparticles, thereby increasing magnetic anisotropy. Increased anisotropy

contributes to heat generation of the nanoparticles during magnetic hyperthermia treatment, and thus this behavior is desirable for this application.

Next, the 50 nm particles with amine coating and 4 wt.% SELP sample is imaged. It can be seen from figure 5.4 below, that chaining of the nanoparticles exists and is similar to the interaction behavior seen in the single dextran coated sample. The nanoparticles tend to chain or cluster together. The dispersion across a wide area is due to the presence of SELP material.

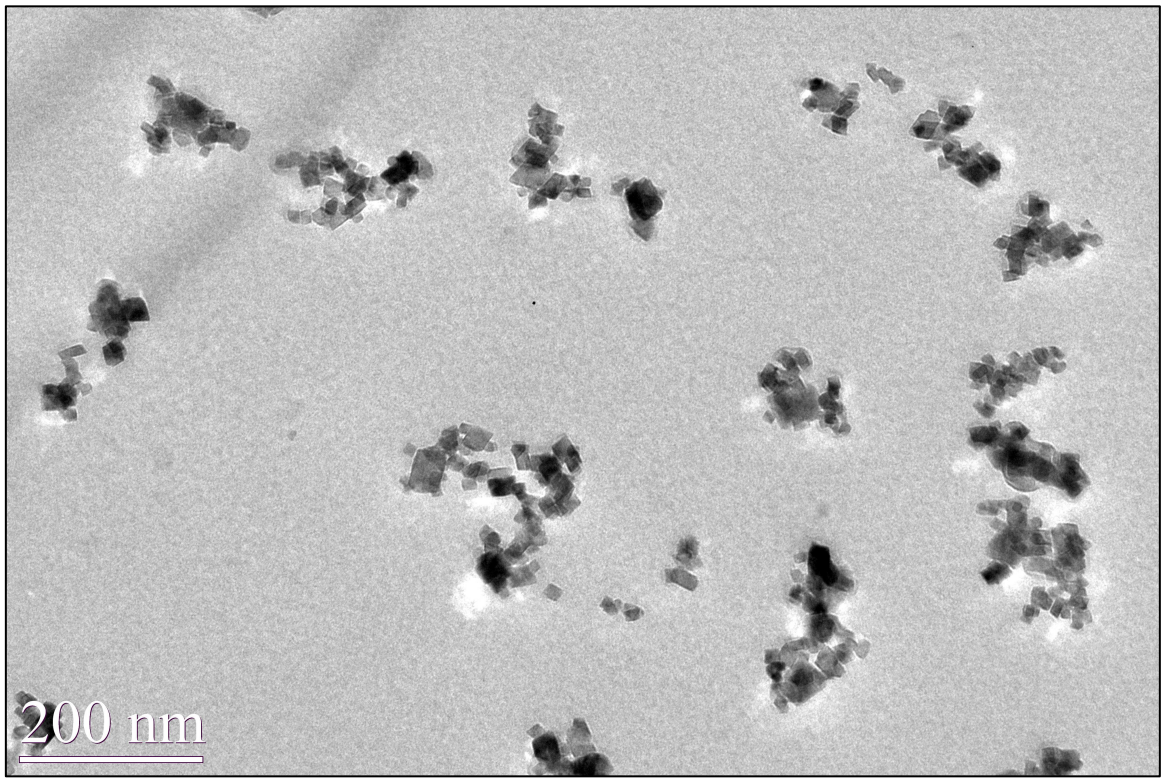

Figure 5.4 TEM of 50 nm nanoparticles with amine coating and 4 wt.% SELP embedded in resin

The TEM images of nanoparticles without SELP showed clustering in small areas, whereas with the addition of SELP, the nanoparticles are dispersed relatively evenly. As seen in the single dextran coated sample prior, by examining the chaining behavior of the

nanoparticles, an outline of a SELP network can be seen. Again, the nanoparticles do not cover the entire SELP network, so an outline of the SELP fibers must be estimated. The average nanoparticle chain is about 100 nm long, with a single nanoparticle around 20 nm wide. The nanoparticle chains range from only a few nanoparticles long, around 75 nm, up to chains as long as 150 nm. Branching of nanoparticle chains is also evident in the TEM image. When the lengths of branches are accounted for, the size of the nanoparticle chains increases. Clusters of nanoparticles can be seen throughout the sample, however chaining is dominant. There seems to be little difference between the amine and single dextran coated nanoparticles when added to SELP polymer. Clusters are present, however they tend to cluster in a linear manner, almost appearing as thick chains that are a few nanoparticles wide. The nanoparticles appear to be chaining along a SELP fiber, however most of the SELP network is not covered by nanoparticles. The disperse nature of the nanoparticles over a large area is the main indication of the presence of SELP.

Lastly, a 50 nm particle with maleimide coating and 4 wt.% SELP sample is investigated in figure 5.5 below. There are immediate differences that are observed when compared to the previous samples of nanoparticles with dextran and amine coats.

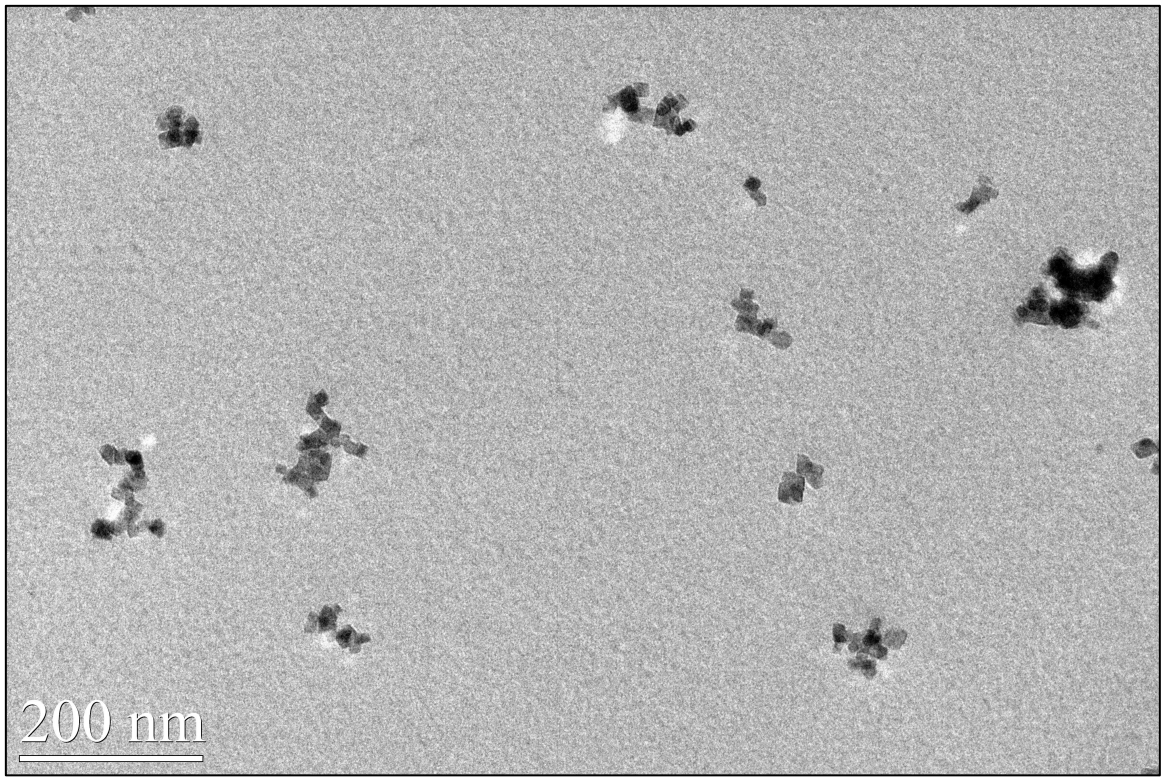

Figure 5.5 TEM of 50 nm nanoparticles with maleimide coating and 4 wt.% SELP embedded in resin

The first observation made is that there seems to be a much lower concentration of nanoparticles in this sample with a maleimide coating. This could be because of coating effects due to the maleimide or simply because the area imaged in the TEM contains a smaller concentration of nanoparticles. There is no evidence of sample settling in the SANS cell. However, even with fewer nanoparticles, there still seems to be evidence of chaining. Most chains are measured to be between 75-125 nm long. A couple small clusters are present, but nanoparticle chaining seems to be the preferred structure. A SELP network is difficult to define, as there are not enough nanoparticle chains to make a clear outline of SELP fibers. The nanoparticles are small, with particles typically around 20 nm in size. This is smaller than the 50 nm nominal diameter, but this is expected. The dispersity of the nanoparticles and existence of chaining indicates that there is SELP

present, even if the nanoparticles do not completely align with the network as evidenced by several small aggregations.

Chaining is evident in all three of the different coatings: single dextran, amine and maleimide. However, chaining is most dominant in the single dextran and amine coated samples. These two samples demonstrate nanoparticles that tend to chain or cluster into a linear manner in which a SELP structure can be identified. By examining a large area of the sample, a SELP network can be determined by looking at where the nanoparticles are aligning. The chaining in the single dextran and amine coated samples demonstrates the effectiveness of these coatings at the 50 nm particle size. The lack of nanoparticles seen in the maleimide coated sample could be due to the steric interactions created between maleimide coats. Another possibility is that the concentration of nanoparticles was low in the sample area that was imaged. SANS measurements will confirm if this is the case.

5.2 Size Comparison

The size of the nanoparticles should have an affect on their chaining behavior in SELP. Ideally, the nanoparticles will be small enough to fit in between the SELP network fibers, yet large enough so that they can interact with the SELP with demixing or precipitating. Three different sizes of nanoparticle diameter are imaged in TEM. Double dextran coated nanoparticles of 30, 50 and 80 nm in hydrodynamic diameter were imaged in 8 wt.% SELP. In figure 5.6 below, the 80 nm particle is presented. A mixture of chaining and clustering is observed.

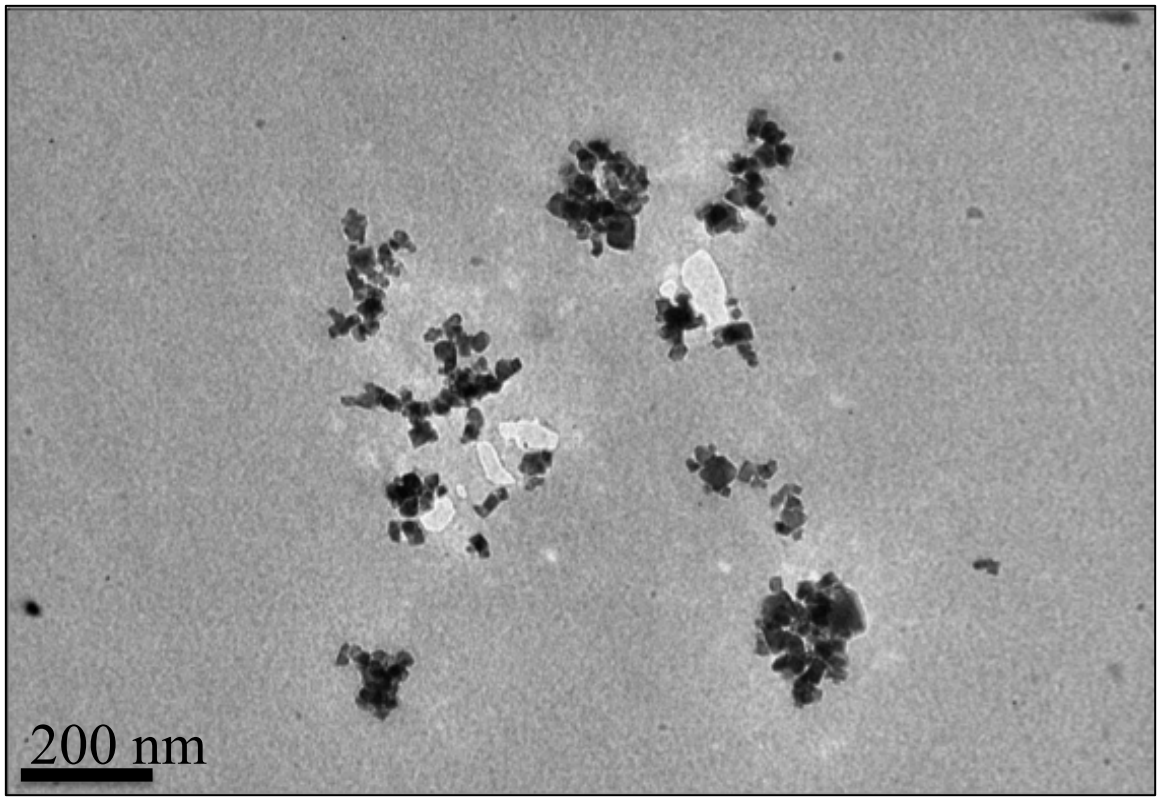

Figure 5.6 TEM of 80 nm nanoparticles with double dextran coating and 8 wt.% SELP embedded in resin

The 80 nm nanoparticles may be able to chain and align along the SELP network. The chains that are seen tend to be a few nanoparticles thick, making it a close distinction between a chain or a cluster. However, mostly nanoparticle clusters can be seen, especially two larger aggregations, one at the top and the other at the bottom of the image. These clusters could be located in a large open area of the SELP network mesh or the large size of the particles could be warping the SELP structure, allowing them to cluster. The clusters are around 100 nm in diameter and comprised of many small nanoparticles. Again, as seen from previous TEM images of the nanoparticles, the hydrodynamic diameter of the nanoparticles is larger than their actual diameter. The nanoparticles seen in figure 5.6 are mostly around 22 nm in diameter, with a few large particles closer to 36 nm, however these larger particles could be multiple overlapping

nanoparticles. These diameters are expected to be smaller than their nominal size found from DLS measurements. From the lack of significant chaining observed, the 80 nm nanoparticles are not an ideal size to interact with the SELP structure.

Microscopy of a 50 nm double dextran coated nanoparticle in SELP sample is seen in figure 5.7 below. Nanoparticle chains are observed alongside several nanoparticle clusters. The nanoparticles seem well dispersed throughout the sample area.

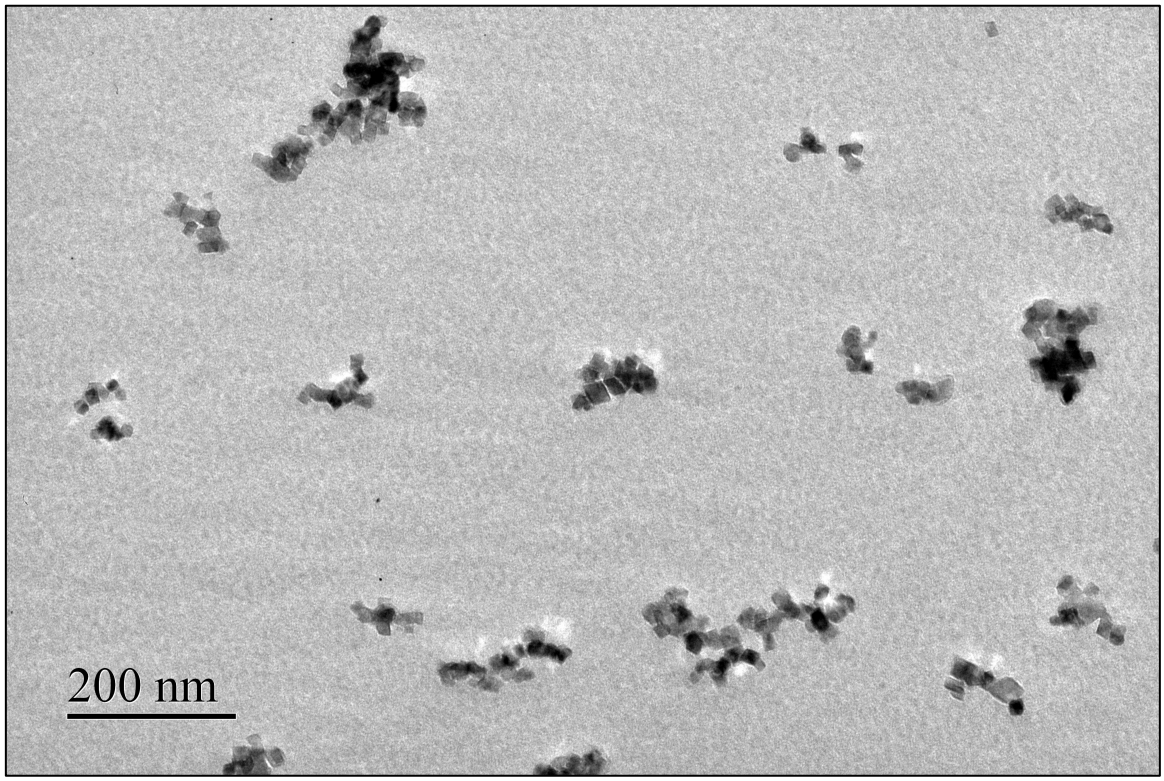

Figure 5.7 TEM of 50 nm nanoparticles with double dextran coating and 8 wt.% SELP embedded in resin.

Clustering is less prominent in the 50 nm nanoparticle size sample when compared to the 80 nm sample. Clusters tend to be around 100 nm in diameter, similar to the 80 nm nanoparticle sample, however there seems to be fewer clusters across a given area. There

are a couple of nanoparticle chains that are a few nanoparticles wide and could be taken for clusters, but still exhibit a longer chaining behavior. However, many of the nanoparticle chains formed are only a few nanoparticles wide and are longer in the 50 nm nanoparticle size than the 80 nm sample. Nanoparticle chains are typically around 175 nm long. A couple of longer chains are observed as well, up to around 250 nm. These longer chains hint that the smaller size nanoparticles are a more appropriate fit within the mesh of the SELP network than the 80 nm nanoparticles, which are likely too large.

In figure 5.8 below, a 30 nm double dextran coated nanoparticle with 8 wt.% SELP sample is imaged. Immediately obvious is the large aggregation of nanoparticles dominating the entire area of the sample imaged.

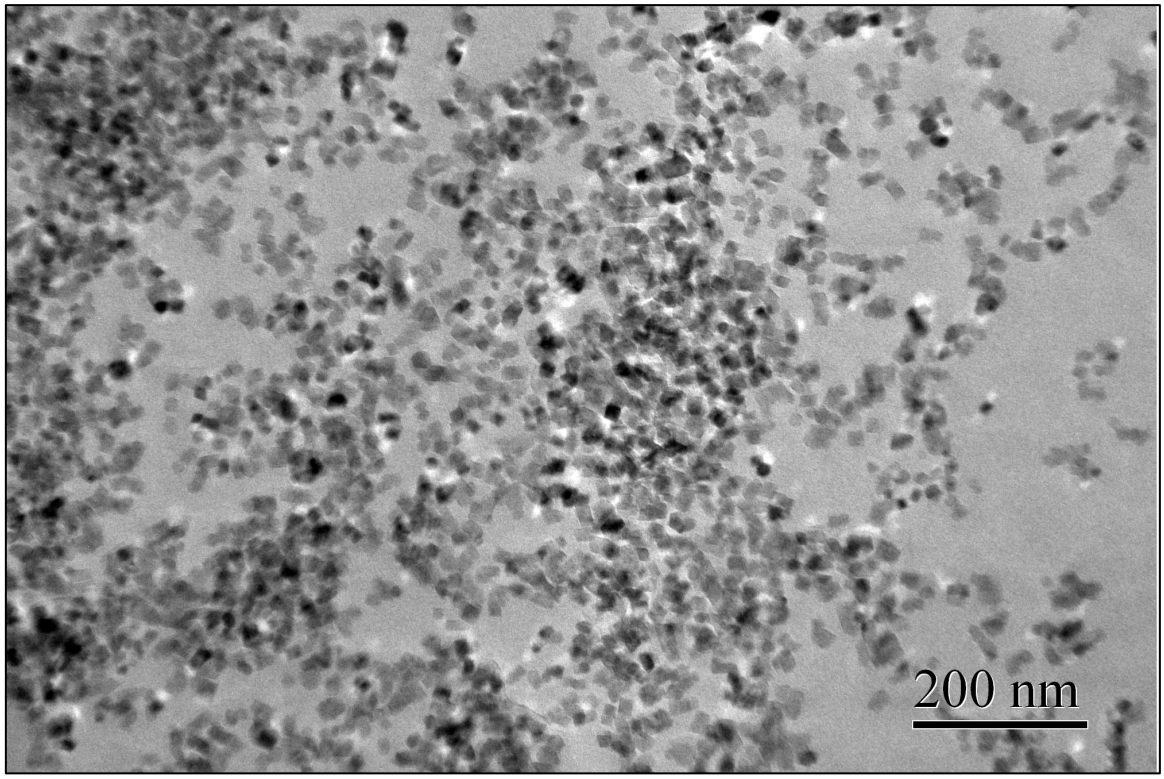

Figure 5.8 TEM of 30 nm nanoparticles with double dextran coating and 8 wt.% SELP embedded in resin

The nanoparticles cluster heavily in this TEM image. There are some smaller clusters and single particles that can be seen, however there are very few obvious nanoparticle chains of significant length. A SELP network cannot be identified from the image. Instead, nanoparticles are clustering in every area of the sample imaged. These 30 nm particles appear to aggregate and strongly cluster and do not disperse throughout the SELP. From the TEM image, the nanoparticles are actually around 20 nm in diameter. They look to be strongly clustered without any regard to an underlying structure of the SELP. These 30 nm nanoparticles could be too small to interact with the 8 wt.% SELP polymer matrix. Further measurements from SANS analysis may help to understand the structure. Comparing the 30, 50 and 80 nm nanoparticle sizes in SELP, chaining is observed in the 50 and 80 nm particle sizes, while the 30 nm nanoparticles only exhibit large scale clustering. While chaining is observed in the two larger particle sizes, the 50 nm particles demonstrate the longest nanoparticle chains and fewest clusters. From the TEM images, the 50 nm nanoparticles seem to interact the most ideally with SELP in terms of chaining behavior and lack of aggregation.

Chapter 6

SANS of Nanoparticles and SELP System

6.1 Introduction

The interaction behavior of the nanoparticles in the SELP polymer was investigated using small angle neutron scattering (SANS). SANS experiments provides scattering data that is reduced using IGOR Pro and SANS software especially created and tailored for the SANS instrument at the Center for Neutron Research at NIST[24]. The SANS data is analyzed to create a graph of scattering wave vector vs. intensity. From this plot, information on the structural features in the sample can be determined.

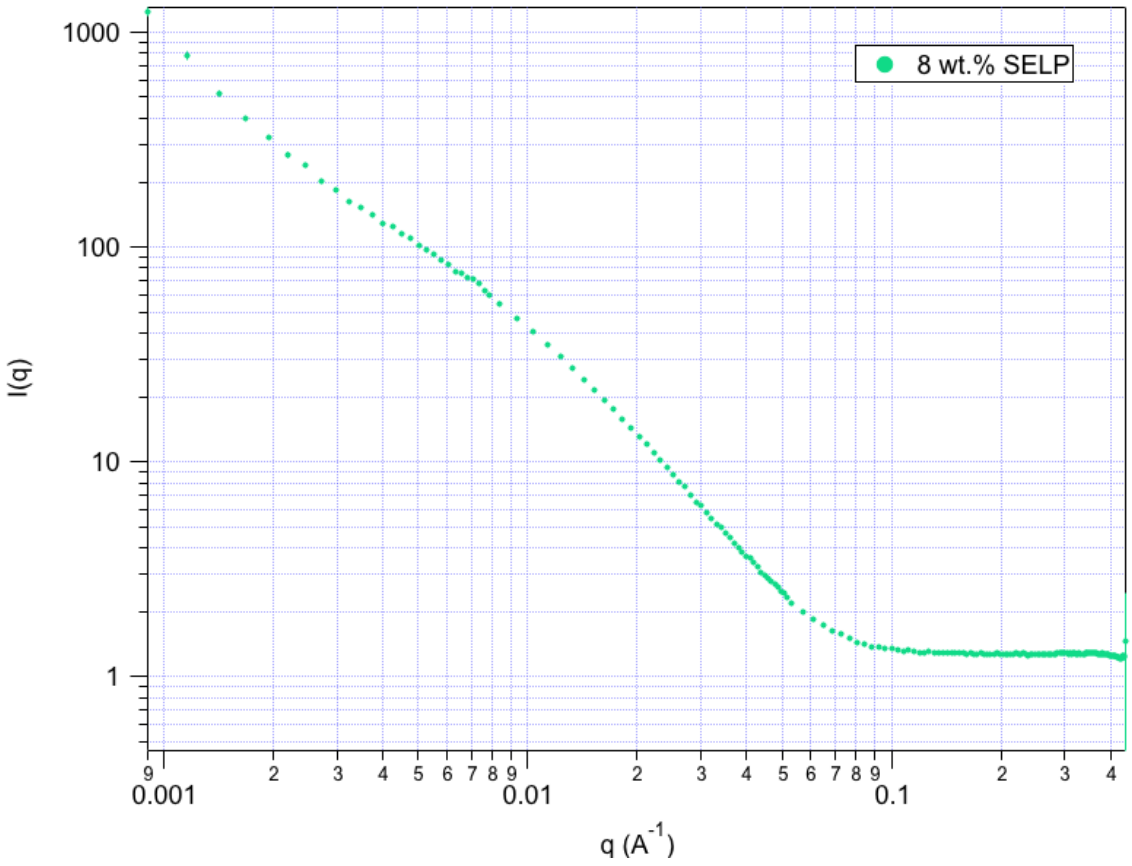

Figure 6.1 SANS plot of 8 wt.% SELP 47K

Figure 6.1 is the scattering of an 8 wt.% SELP sample with no nanoparticles. A SELP only sample can be measured in SANS and then subtracted as background from the nanocomposite samples to find nanoparticle structure while in a SELP matrix. In order to quantify the SANS data, an appropriate fitting model must be used. The SANS data was quantified by using a flexible cylinder model which is used to describe relatively stiff chain-like objects. Thus, each nanoparticle chain will be identified in terms of chain segments. From the parameters of the model, we can try to gain insight into whether the nanoparticles are stiff chain segments, single nanoparticles or a different structure within SELP. The contour length describes the length of the entire nanoparticle chain, while the Kuhn length measures the length of a rigid segment of a nanoparticle chain. The diameter of the nanoparticle segment and the number of nanoparticles in a nanoparticle chain are calculated from the given fitting parameters. A schematic of the flexible cylinder model is seen below in figure 6.2[30].

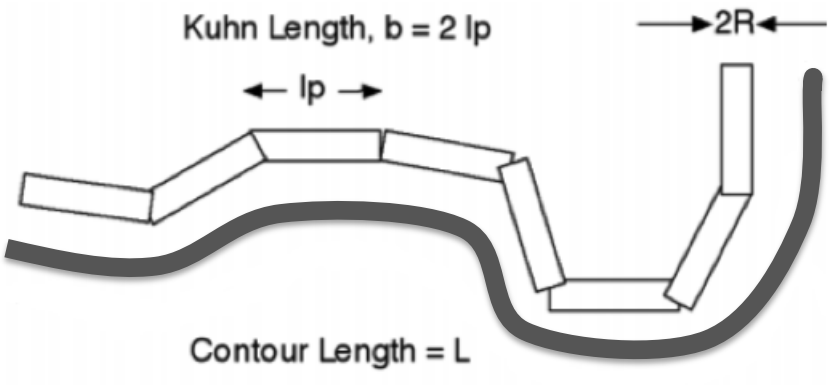

Figure 6.2 Schematic of flexible cylinder model

Ideally, the samples will follow the flexible cylinder model if nanoparticle chaining exists. Clustering is not represented in this model, but as seen from the TEM images,

appears to occur in many of the samples. How the model treats and represents the clusters will be interesting to examine. The same series of samples will be investigated through SANS measurements and analysis: a comparison of different functionalization of the nanoparticle coating, size comparison and SELP concentration series.

6.2 Coating Comparison

Applying the flexible cylinder model to the SANS data of the nanoparticle/SELP nanocomposite system, we can compare nanoparticle chaining between samples. Nanoparticle samples with three different coatings, single dextran, amine or maleimide, were investigated for 50 nm particles all with 4 wt.% SELP. In figure 6.3, the blue points represent the neutron scattering data, while the red and black lines represent the flexible cylinder model fit of the data. The points are plotted on a logarithmic scale as wave vector, q, (A^{-1}) versus scattering intensity (cm^{-1}). The flexible cylinder model fits moderately well for the sample. There are a couple of areas where the model does not completely fit the sample scattering. At low q, long range size structure is not completely represented by the flexible cylinder model and at high q, where a structural feature at about q = 0.06 $Å^{-1}$ does not quite fit.

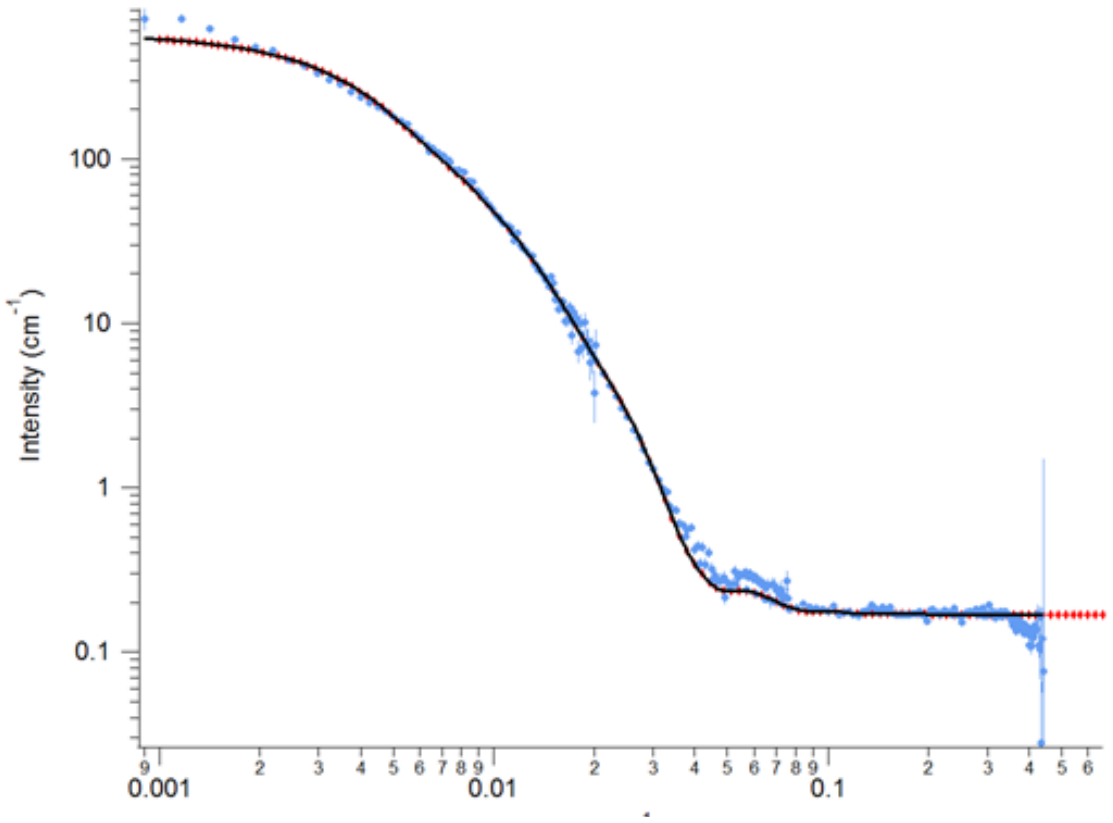

Figure 6.3 SANS fit of 50 nm nanoparticles with single dextran coat and 4 wt.% SELP

Contour Length	204 nm
Kuhn Length	71 nm
Diameter	43 nm
Number of Particles in Chain	5

Table 6.1 Flexible cylinder model parameters for 50 nm nanoparticles with single dextran coat and 4 wt.% SELP

Table 6.1 above, contains the parameters attained from fitting the sample to a flexible cylinder model. The diameter of the nanoparticle chain, or the cylinder in this model, was found to be 43 nm. This is slightly smaller than the 50 nm diameter measured through DLS. This value is reasonable due to the fact that the DLS gives a hydrodynamic diameter, which is expected to be larger due to the expansion of dextran in solution. The

Kuhn length describes the size of the stiff chain segments, which seems to be approximately two nanoparticles in length. The contour length, which describes the entire length of the nanoparticle chain, is 204 nm. From these values, the total number of nanoparticles in a chain can be estimated. In the case of the 50 nm single dextran coated nanoparticles with 4 wt.% SELP sample, each nanoparticle chain is around 5 nanoparticles in length. This nanoparticle chain size seems small in comparison to the chains that were observed from the TEM image (figure 5.1) of the same sample. While there is some chaining in this range, there are many more branches and clusters that the flexible cylinder model may not be best suited to fit. Since the model is based conceptually on a polymer chain, it may not be able to appropriately account for the nanoparticle clusters. Some of the branched nanoparticle chain segments could be modeled properly through the Kuhn length measurement, but others may be examined as a separate nanoparticle chains, which would explain the short nanoparticle chain length given by the fitting parameters. Also the effect of the heavy overlapping of the nanoparticles, as seen in the TEM image, on the model parameters should be considered. If two nanoparticles are closely overlapped, SANS and the flexible cylinder model may not separate these two nanoparticles, but instead treat them as a single particle. The size of a single nanoparticle, as seen in the TEM image, figure 5.1, is about 20 nm. This value is smaller than the 43 nm obtained from SANS fitting. If the number of nanoparticles in a chain is calculated using the 20 nm diameter from TEM, the length of the chain increases to 10 particles from 5 particles with the SANS derived diameter. The TEM diameter value will not include the dextran coating, while the DLS calculated diameters do. This accounts for the smaller particle size obtained from the TEM images, when compared to

the DLS sizes. The SANS diameter value is dominated by the iron oxide core of the nanoparticles, thus the dextran coatings will again play a minimal role in the particle sizes derived from SANS model fitting. It is also possible that multiple nanoparticles are being measured from the fitting. This would give longer chains with more nanoparticles, and is consistent with what is observed in the TEM image of the same sample. Chains vary widely between 75-250 nm long. The nanoparticle chains are not exclusively linear, but tend to bend in a different direction every 50 nm or so. There are also some shorter nanoparticle chains, which are only a few nanoparticles long. This double dextran coated nanoparticle sample can be compared with the following amine coated nanoparticle sample in 4 wt.% SELP in figure 6.4.

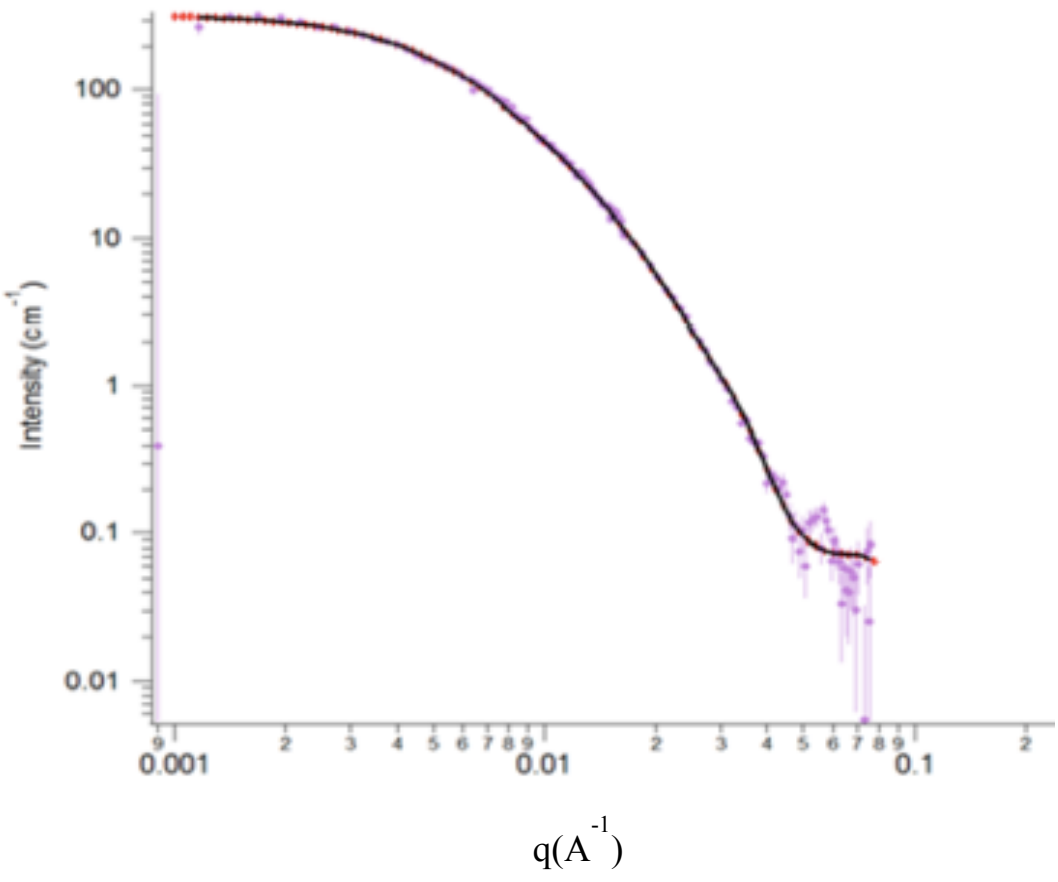

Figure 6.4 SANS fit of 50 nm nanoparticles with amine coating and 4wt.% SELP

At low q, the model fits nicely with the long range structures in the sample. These low q features are likely to be nanoparticle chains. However, at high q, the flexible cylinder model cannot accurately fit the high q feature that is seen above as a peak in the data points. This feature could be related to the diameter of the cylinder from the model. Fitting the sample with the flexible cylinder model and calculating the parameters, gives table 6.2 below.

Contour Length	273 nm
Kuhn Length	17 nm
Diameter	34 nm
Number of Particles in Chain	8

Table 6.2 Flexible cylinder model parameters for 50 nm nanoparticles with amine coat and 4 wt.% SELP

The diameter of the nanoparticle is 34 nm, which is smaller than the nominal 50 nm size, as expected. This correlates with the previous 50 nm double dextran coated sample. The Kuhn length for this sample is smaller than the diameter of a particle, which is interesting and not expected. With the Kuhn length being about half the diameter of a nanoparticle, it is possible that the model is measuring more than one nanoparticle. However, from TEM imaging of this sample, figure 5.4, the diameter is about 20 nm, which is close to the 17 nm Kuhn length. Thus each Kuhn segment is likely measuring one nanoparticle. Other models should be considered for this sample since the Kuhn length is too short to be physically reasonable. However, examining other models is not in the scope of this research project. From the model parameters, the contour length is found to be 273 nm, which gives an average nanoparticle chain length of around 8 particles. However, if each nanoparticle is actually closer to the Kuhn length of 17 nm, then the number of nanoparticles in a chain increases to 16. The SANS fitted data supports what is observed

from the TEM image of this sample. Mostly nanoparticle chains exist in this sample, with a few examples of clustering scattered throughout. The amine coating seemed to slightly increase the amount of chaining observed in the sample when compared to the double dextran sample. The flexible cylinder model also seems to be a good fit when examining the low q range structures. However, it does not fit properly to high q features seen on the SANS graph. Most of the SANS fits studied seem to have difficulty in modeling this high q structure which could be representative of attempts to fit the radius of the flexible cylinder. Finally, to complete the coating series, a 50 nm nanoparticle with maleimide coating and 4 wt.% SELP sample is plotted below with the flexible cylinder fit shown.

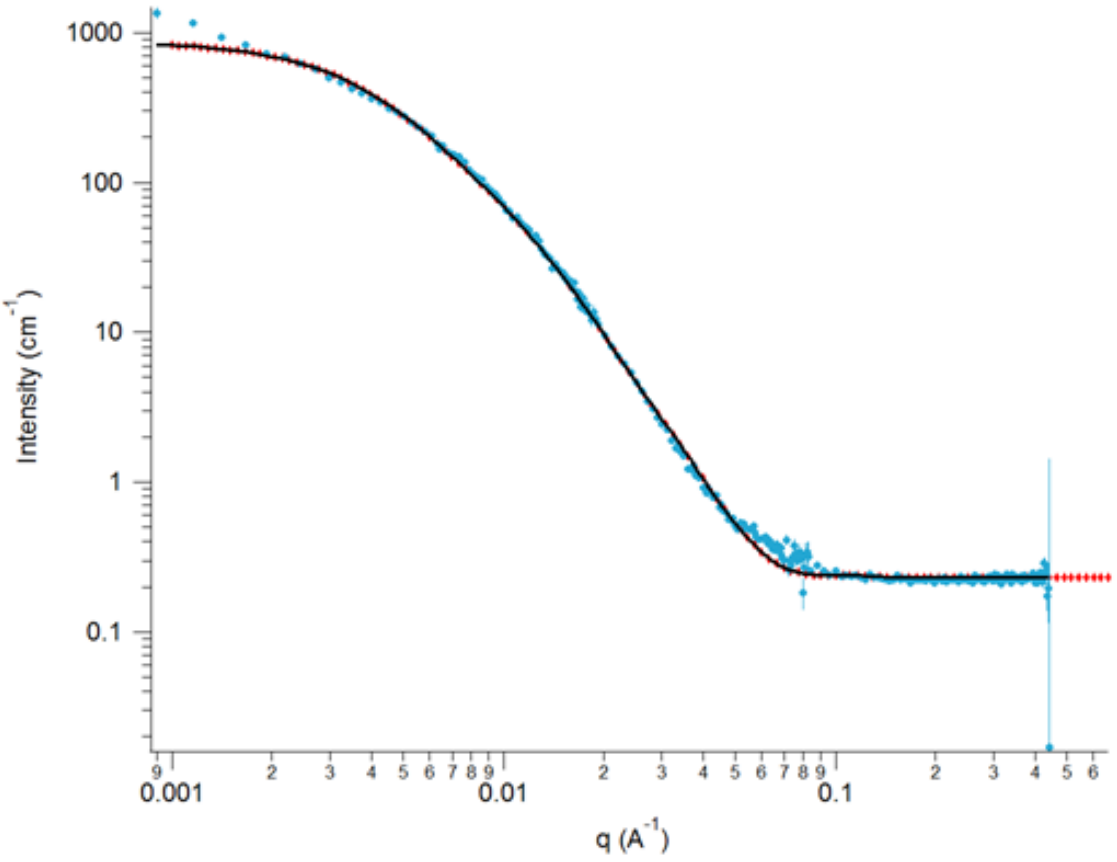

Figure 6.5 SANS fit of 50 nm nanoparticles with maleimide coating and 4 wt.% SELP

Similar to the double dextran coated sample, the flexible cylinder model has some trouble with completely fitting large range structures seen at high q. It is likely that some of the poor fit may be due to clustering of the nanoparticles or splicing of the low q and high q data from the different detector settings. There is also a slight bump around 0.6 A^{-1} that the model doesn't quite fit, although this feature does not seem as intense in the maleimide coated sample as seen from prior samples. Otherwise, the flexible cylinder model seems to be a reasonably accurate model for fitting the nanoparticle chains. Below, table 6.3, holds the fitting parameters as calculated through using the flexible cylinder model.

Contour Length	808 nm
Kuhn Length	8 nm
Diameter	32 nm
Number of Particles in Chain	25

Table 6.3 Flexible cylinder model parameters for 50 nm nanoparticles with maleimide coat and 4 wt.% SELP

The diameter from the model parameters is similar to the amine coated sample, which is expected, as the nanoparticles should be the same size. In this sample, the Kuhn length is about 25% the diameter of a nanoparticle. This is even smaller than what was observed for the Kuhn length in the amine coated sample. If the Kuhn length is actually a closer representation of the nanoparticle diameter, 8 nm seems incredibly small. As seen from the microscopy image of this sample (figure 5.5), the nanoparticles were around 20 nm in diameter. However, single particle identification is difficult and multiple overlapping nanoparticles could be mistaken for one nanoparticle. The contour length is 808 nm, giving chains that are approximately 25 nanoparticles long with the flexible cylinder model diameter of 32 nm being used to calculate the length. If the nanoparticles are

indeed smaller than 32 nm, and closer to the 20 nm TEM derived diameter, then the number of nanoparticles in this chain increases to 40. Although, it is important to note that these nanoparticles tend to chain when they are present in the TEM imaged area. Perhaps the area that was imaged in the TEM has a smaller concentration of nanoparticles. SANS measures the bulk sample, meaning that what may not have been observed in the TEM, was measured by SANS. This could give longer nanoparticles chains or more clusters that are not seen from just examining the sample in the TEM.

6.3 Size Comparison

A size series comparing the 50 and 80 nm nanoparticles nominally in diameter with double dextran coat and 8 wt.% SELP was examined using SANS and fit using the flexible cylinder model. Figure 6.6 below, is an 80 nm nanoparticles in double dextran coating with 8 wt.% SELP sample.

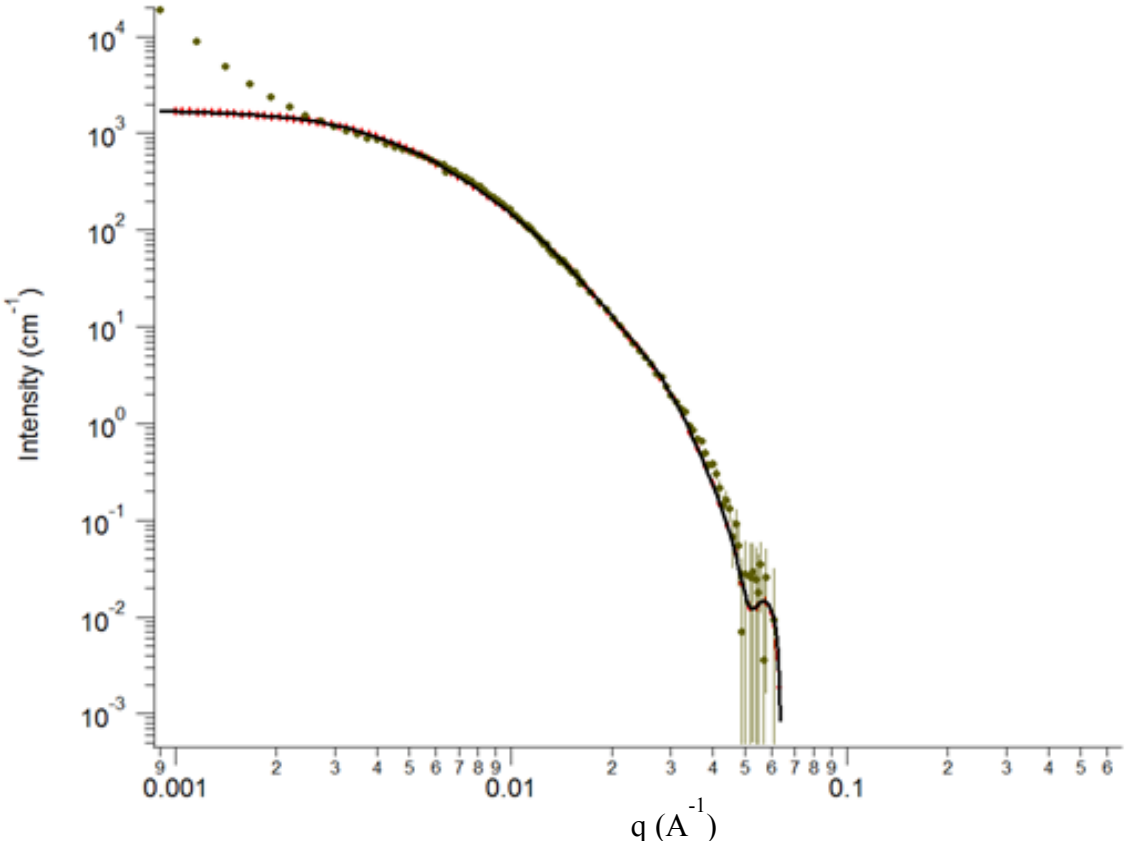

Figure 6.6 SANS fit of 80 nm nanoparticles with double dextran coating and 8 wt.% SELP

As seen in the graph, the flexible cylinder model does not follow the increased scattering at low q. While the flexible cylinder model levels off, the scattered intensity continues increasing, indicating the presence of large range structures and aggregation. Clustering is observed in the TEM image of this sample, which is consistent with the low q scattering. It is likely that chaining is not dominant in this sample. Particles appear to either stay dispersed or aggregate into large clusters. The VSM measurements also suggest clustering from the coercivity observed, especially from the 80 nm nanoparticle samples.

Contour Length	473 nm
Kuhn Length	11 nm
Diameter	42 nm
Number of Particles in Chain	11

Table 6.4 Flexible cylinder model parameters for 80 nm nanoparticles with double dextran coat and 8 wt.% SELP

In table 6.4 above, the fit parameters for this sample reveal moderate chaining of the nanoparticles. The average number of particles in a chain is eleven. This value correlates with the chaining seen in the TEM image, figure 5.6, of the same sample. The diameter of 42 nm is smaller than the 80 nm hydrodynamic diameter, but this difference is expected as it has been seen in all the previous samples. The TEM observed diameter is 22 nm, making nanoparticle chains 22 particles long. Some larger nanoparticles or possibly overlapped particles of approximately 36 nm were observed in the TEM. This estimation is in the same range as the SANS value of 42 nm nanoparticles. The Kuhn length of 11 nm is relatively small to that observed by the TEM. It may be that although the model fits the SANS data it is not an accurate description of this sample. Alternatively, because the diameter of the nanoparticles is larger than the Kuhn length, this may suggest that the TEM measured diameter of a nanoparticle is actually for multiple particles. This supports the theory of clustering in this sample as observed in TEM, VSM and now SANS.

The SANS data for the 50 nm nanoparticle with double dextran coating and 8 wt.% SELP is shown in figure 6.7. Table 6.5 gives the model fit parameters for this sample.

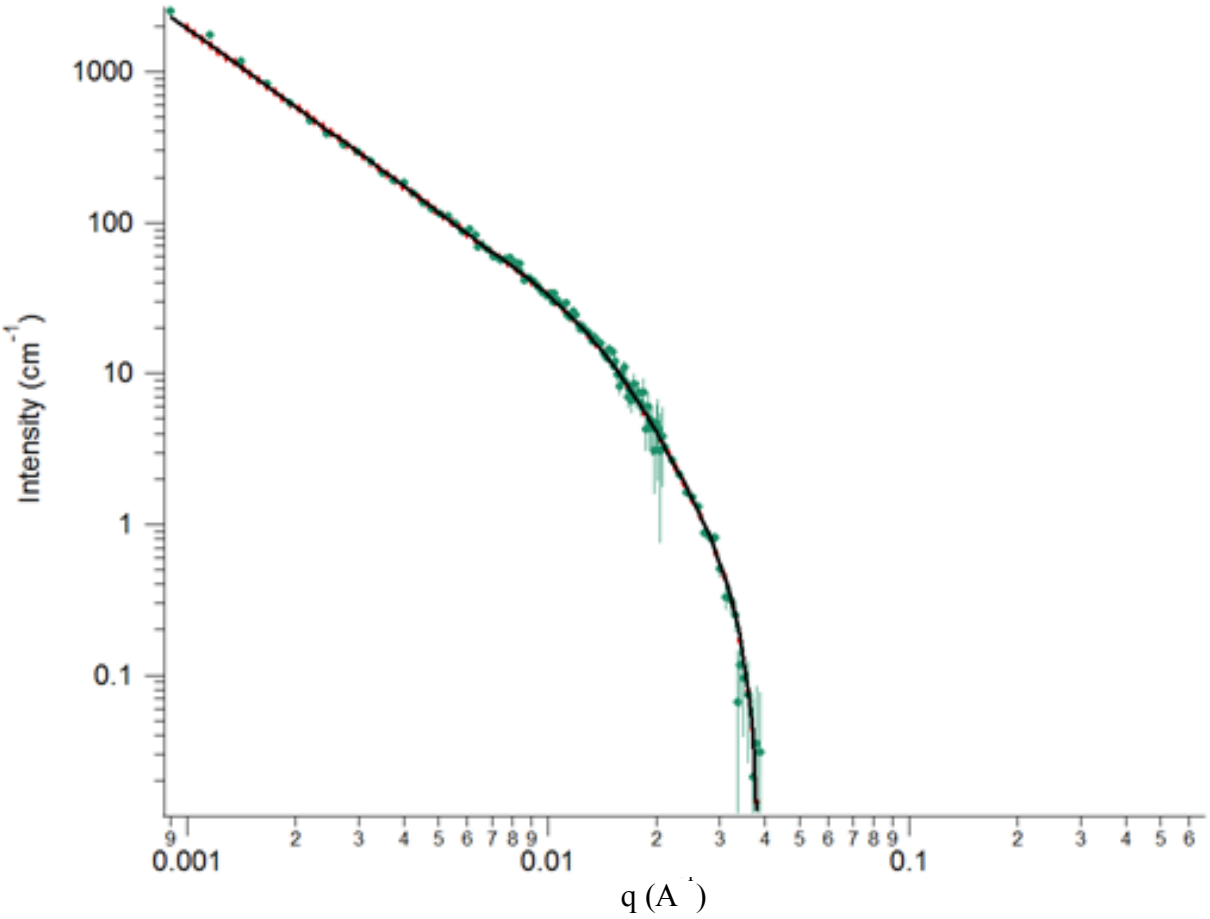

Figure 6.7 SANS fit of 50 nm nanoparticles with double dextran coating and 8 wt.% SELP

Contour Length	6109 nm
Kuhn Length	59 nm
Diameter	37 nm
Number of Particles in Chain	165

Table 6.5 Flexible cylinder model parameters for 50 nm nanoparticles with double dextran coat and 8 wt.% SELP

For the 50 nm nanoparticle sample the number of particles in a chain is 165. The contour length of the chain is extremely long when compared to the other samples that have been

examined. The flexible cylinder fit parameters seem to indicate that there is very long chaining occurring within the sample. Chains that are 6,109 nm in length would be very easy to spot, however from the TEM images of this sample (figure 5.7), chains of this length are not observed. There is chaining in the sample, however not as long as suggested by the model parameters. However, SANS does measure the bulk sample, while the TEM can only image a small section. It is possible that there are incredibly long chains elsewhere on the sample that were not imaged by the TEM or that the long chains were broken during TEM sample preparation. If the chains are not in plane with the direction of microtoming, then they would be disrupted during sample preparation. VSM data of this sample, as seen in table 4.1, suggests smaller coercivities, less anisotropy and less clustering when compared to the 80 nm nanoparticle samples. The Kuhn length and diameter parameters are reasonable. The Kuhn length describes rigid chain segments or branches of around two nanoparticles long. In figure 6.8 below, an example of nanoparticle chain branching is demonstrated. This type of branching can account for Kuhn lengths of only a couple of nanoparticles long. These branches could possibly be representing an underlying SELP structure of crosslinking points and polymer fibers.

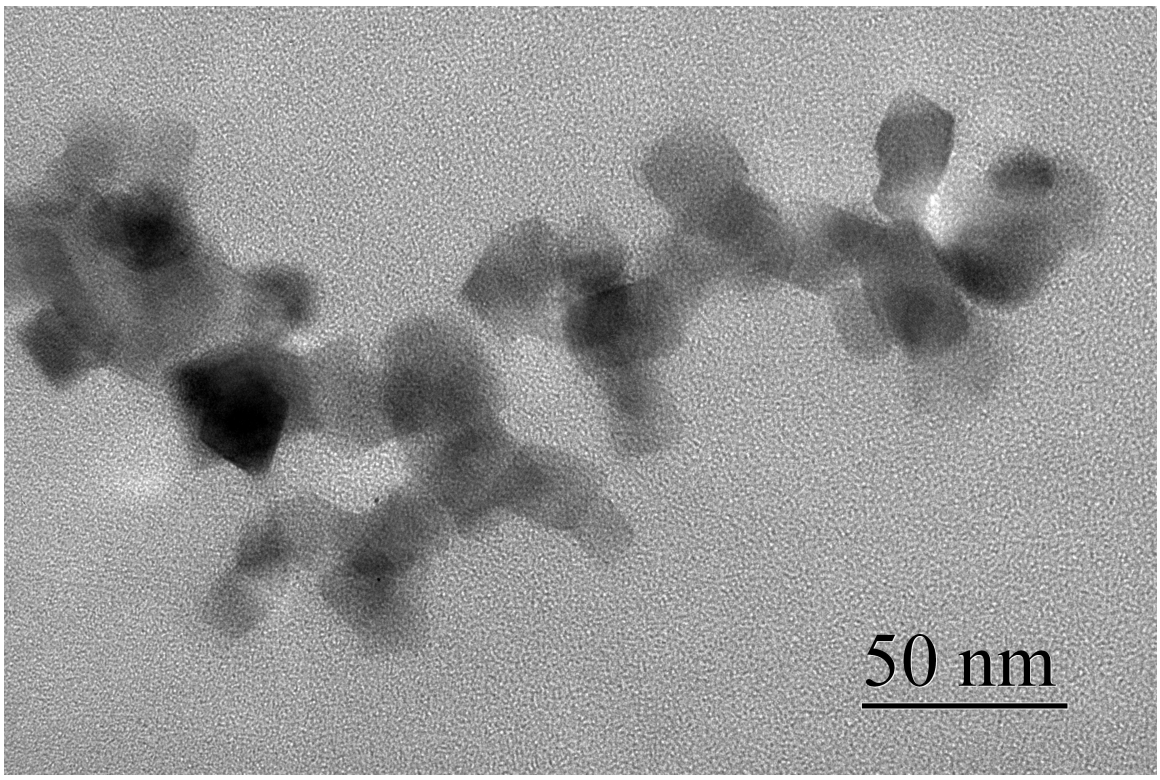

Figure 6.8 TEM of 50 nm nanoparticles with double dextran coating and 8 wt.% SELP

A diameter of 37 nm is in the same range as the DLS hydrodynamic diameter of 50 nm. This double dextran coated, 50 nm nanoparticle with 8 wt.% SELP may offer the most chaining for any sample.

The optical microscopy image in figure 6.9 shows the large amounts of intensity of nanoparticle clustering in a 30 nm nanoparticle with double dextran coating and 8 wt.% SELP sample taken after SANS measurements. This could be due to drying effects, however this was the only sample that demonstrated heavy aggregations. By observation of the sample in the SANS sample cell, it was apparent that the nanoparticles had settled to the bottom of the cell. As a result of this, the background measurements for this sample are wrong, making the SANS data unusable. There is no information about nanoparticle distribution in SELP material.

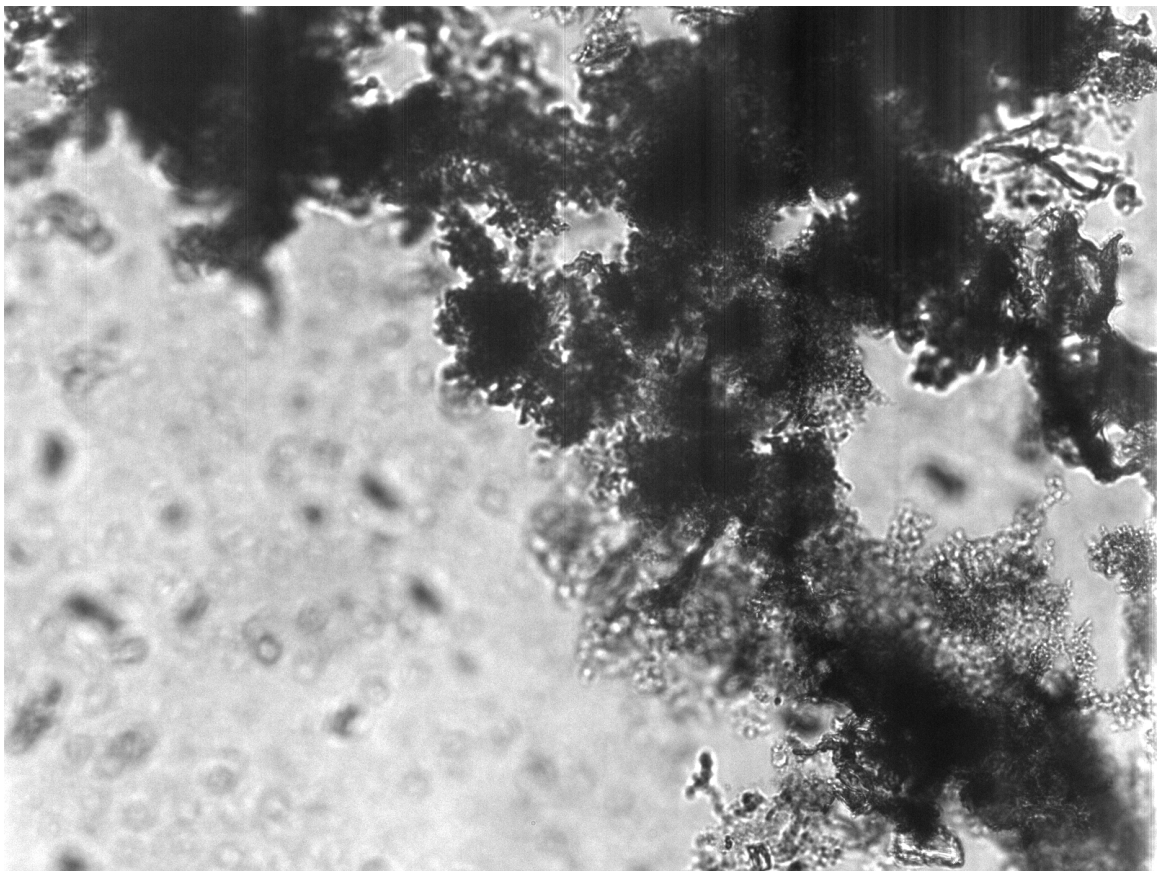

Figure 6.9 Optical microscopy of 30 nm nanoparticles with double dextran coating and 8 wt.% SELP SANS sample

Since the nanoparticles settled to the bottom of this sample, they are not interacting with the SELP fibers. Other samples demonstrated strong clustering but always remained suspended in the sample. This 30 nm nanoparticle sample showed the strongest evidence of particles that completely separated from the SELP structure. The nanoparticles were not dispersed within the polymer and did not remain in SELP after gelation, as would be expected. One possibility was that the 30 nm nanoparticles are too small to remain trapped and stay within the SELP gel fiber structure. Instead of interacting with the structure, they simply fall through the network and settle collectively at the bottom of the sample. This behavior explains why the SANS experiment failed to yield usable data on this sample.

As observed from the TEM image (figure 5.8) and optical microscopy (figure 6.9) of the SANS sample, the 30 nm nanoparticles are too small to remain in the polymer network mesh, whereas the 50 and 80 nm nominal nanoparticles are large enough to interact with SELP. The fitting parameters of the flexible cylinder model suggest that the sample with 50 nm sized nanoparticles exhibits the longest chains. The 80 nm nanoparticle sample demonstrates moderate chaining, however when compared to the 50 nm nanoparticle sample, the increased size of the particles could negatively affect its chaining behavior. The 80 nm particles may have a difficult time fitting into the polymer network depending on the mesh size between the polymer fibers. If the nanoparticles are too small, then they simply fall out of the SELP gel structure altogether. This demonstrates the effect that size of the nanoparticles has on the chaining behavior of the overall nanoparticle-SELP nanocomposite system.

Chapter 7

7.1 Conclusion

From the various characterization techniques of DLS, VSM, TEM and SANS, some aspects of the nanoparticle and SELP nanocomposite system can be understood. The sizes of the nanoparticles are found to be smaller than their nominal DLS diameters through TEM and SANS analysis. This result was expected because DLS measures a hydrodynamic diameter of the nanoparticles, not the dry nanoparticle size. VSM measurements revealed ferromagnetic behavior in the nanocomposite samples that increases with increasing nanoparticle diameter, as well as different levels of magnetism found between samples of different coatings. The single dextran sample coated nanoparticles had the greatest interparticle interactions, while the double dextran, amine and maleimide coated nanoparticles have smaller amounts of magnetic interactions. TEM imaging revealed both clustering and chaining of the nanoparticles in SELP. The various coating on the samples did not have as much of an effect on their dispersion in a SELP network as the size variations of the nanoparticles did. The amount of chaining or clustering observed was influenced by nanoparticle sizes in 8 wt.% SELP samples. The 30 nm nanoparticles were too small to be able to integrate with the SELP network properly and precipitated out of the sample. The 80 nm nanoparticles were not stable with SELP and may be too large to fit within the mesh size of the 8 wt.% SELP network. The 80 nm nanoparticles demonstrated minimal chaining. However, the 50 nm nanoparticles typically formed nice, long chains around 175 nm. Clustering was still present, however minimal. The affect of the concentration of SELP on the nanoparticles in polymer was more difficult to decipher. Overall, there were no obvious differences between the two.

SANS measurements confirmed what was observed from VSM experiments about the various nanoparticle coatings. The single dextran coated nanoparticles, with only the exception of one sample, all had the smallest chain lengths after fitting with the flexible cylinder model. The maleimide coated nanoparticle-SELP nanocomposite samples typically had the longest nanoparticle chains, as calculated with the flexible cylinder model fit. The size of the samples was also determined through SANS to affect the nanoparticle-SELP interactions, confirming what was observed in the VSM and TEM experiments. From flexible cylinder fits, the 50 nm nanoparticles samples had the longest chains, at 165 nanoparticles long. Comparing the SANS data between 4 wt.% and 8 wt.% SELP, the 8 wt.% sample gives longer nanoparticle chains, which actually contradicts what is found through TEM imaging. In SANS, the 4 wt.% SELP sample gives nanoparticle chains of 14 nanoparticles long, while the 8 wt.% SELP samples have 35 nanoparticle long chains. However, in TEM, the 4 wt.% SELP samples tend to have better nanoparticle chaining than the 8 wt.% samples. The discrepancy could be due to local variations in the TEM sample. From the materials characterization of DLS, VSM, TEM and SANS techniques, the structural and magnetic properties of the Fe_3O_4 nanoparticle-SELP nanocomposite systems could be determined for the advancement of hyperthermia therapy applications. The size and surface coating of the nanoparticles played a large role in a sample's magnetism and interactions with the SELP polymer material. The affect of the SELP concentration in a sample is not as apparent and may not have a significant difference on samples. All of these nanoparticle and SELP network parameters need to be considered when designing the ideal nanocomposite system for use in biomedical applications. The Fe_3O_4 nanoparticle-SELP nanocomposite systems

demonstrated significant nanoparticle chaining and magnetism, both desired properties for a good hyperthermia therapy system.

7.2 Future Work

This section reviews several suggestions for future work. These experiments include additional TEM, atomic force microscopy (AFM) measurements, additional nanoparticle sizes and SELP concentrations, and *in vivo* testing of the nanocomposite system. Some the samples had contradictory results from SANS and TEM, for example, the 50 nm maleimide coated nanoparticles and 4 wt.% SELP. TEM imaging showed only a few nanoparticle chains, while SANS fits calculated that maleimide had the longest chains out of all the nanoparticle coatings. Additional experiments should be done on this sample to identify the discrepancy between the TEM and SANS results. Imaging of both the nanoparticles and SELP would also be something to examine. TEM has been performed on the nanoparticles and SELP separately, however so far imaging the nanoparticles in the SELP network has proven to be difficult. Embedding the samples in an epoxy through an exchange process or staining of the sample to improve contrast, would be possible methods. Atomic force microscopy (AFM) can be utilized to examine the nanoparticle/SELP nanocomposite system in both dry and wet conditions. The sizes of the nanoparticles can be determined and compared to the sizes measured between DLS and TEM. AFM measures the contours of a sample surface by the deflections of a cantilever interacting with the surface. AFM measurements on a similar SELP system have already been completed[12], and ideally, the nanocomposite system will be imaged. AFM has both dry and wet imaging capabilities, allowing size measurements of the nanoparticles, dried and infiltrated with water, to be measured and compared with size

measurements from DLS and TEM. In this thesis, only nanoparticles of 30, 50 or 80 nm are examined. It was shown that 30 nm is too small to interact with SELP and 80 nm is too large and tends to cluster. However, other nanoparticle sizes in between 30 and 80 nm could potentially be ideal sizes for interaction with SELP. Only 4 and 8 wt.% SELP was used in these experiments, however it is known that the gelation window of SELP is between 4 and 12 wt.%. It is possible that the different mesh sizes that are present in these concentrations of SELP will interact differently with various nanoparticle sizes. For example, the 30 nm nanoparticles tended to precipitate out of the SELP gel but it is possible that a 12 wt.% SELP concentration would have a mesh small enough to retain the 30nm nanoparticles. In addition to changing the SELP concentration, the SELP chemistry can be altered as well. SELP 47K was used in these experiments, however there are other SELP block ratios such as SELP 815K which consists of 8 silk units and 15 elastin units. This altered structure will likely have an impact on how nanoparticles interact with the SELP network. Additionally, multiple VSM measurements of the nanocomposites should be taken to ensure accuracy and reproducibility of the values obtained. The values measured in the VSM were only measured once; multiple measurements will be able to confirm the findings. Finally, *in vivo* testing would be a natural progression for this research. The nanoparticles have previously been tested using mouse models, however they have not been tested after being embedded in SELP. The heat generation of the nanoparticles in SELP could be tested and compared to previous trials of just the nanoparticles. Ideally, with the addition of SELP, the heat generation would remain the same or increase from the added anisotropy that the SELP structure provides the nanoparticles.

8. References

1. Dennis, C.L., Jackson, A. J., Borchers, J. A., Hoopes, P.J., Strawbridge, R., Foreman A.R., van Lierop, J., Grüttner, C., Ivkov, R. "Nearly complete regression of tumors via collective behavior of magnetic nanoparticles in hyperthermia". *Nanotechnology* **20**, 395103 (2009).

2. Gilchrist, R.K., Medal, R., Shorey, W.D., Hanselman, R.C., Parrott, J.C., Taylor, C.B. "Selective inductive heating of lymph nodes". *Annals of surgery* **146**, 596-606 (1957).

3. Moroz, P., Jones, S.K., Gray, B.N. "Magnetically mediated hyperthermia : current status and future". *International Journal of Hyperthermia* **18**, 267-284 (2002).

4. Sonvico, F., Mornet, S., Vasseur, S., Dubernet, C., Jaillard, D., Degrouard, J., Hoebeke, J., Duguet, E., Colombo, P., Couvreur, P. "Folate-conjugated iron oxide nanoparticles for solid tumor targeting as potential specific magnetic hyperthermia mediators: synthesis, physicochemical characterization, and in vitro experiments". *Bioconjugate chemistry* **16**, 1181-8 (2005).

5. Hayashi, K., Moriya, M., Sakamoto, W., Yogo, T. "Chemoselective Synthesis of Folic Acid-Functionalized Magnetite Nanoparticles via Click Chemistry for Magnetic Hyperthermia". *Chemistry of Materials* **21**, 1318-1325 (2009).

6. Zhang, J.L., Srivastava, R.S., Misra, R.D.K. "Core-shell magnetite nanoparticles surface encapsulated with smart stimuli-responsive polymer: synthesis, characterization, and LCST of viable drug-targeting delivery system". *Langmuir : the ACS journal of surfaces and colloids* **23**, 6342-51 (2007).

7. Gupta, A.K., Naregalkar, R.R., Vaidya, V.D., Gupta, M. "Recent advances on surface engineering of magnetic iron oxide nanoparticles and their biomedical applications". *Nanomedicine (London, England)* **2**, 23-39 (2007).

8. Carmen Bautista, M., Bomati-Miguel, O., del Puerto Morales, M., Serna, C.J., Veintemillas-Verdaguer, S. "Surface characterisation of dextran-coated iron oxide nanoparticles prepared by laser pyrolysis and coprecipitation". *Journal of Magnetism and Magnetic Materials* **293**, 20-27 (2005).

9. Hong, R.Y., Feng, B., Chen, L.L., Liu, G.H., Li, H.Z., Zheng, Y., Wei, D.G. "Synthesis, characterization and MRI application of dextran-coated Fe3O4 magnetic nanoparticles". *Biochemical Engineering Journal* **42**, 290-300 (2008).

10. Dennis, C.L., Jackson, A. J., Borchers, J. A., Ivkov, R., Foreman, A.R., Hoopes, P.J., Strawbridge, R., Pierce, Z., Goernitz, E., Lau, J.W., Grüttner, C. "The influence of magnetic and physiological behaviour on the effectiveness of iron oxide nanoparticles for hyperthermia". *Journal of Physics D: Applied Physics* **41**, 134020 (2008).

11. McCarthy, J.R., Weissleder, R. "Multifunctional magnetic nanoparticles for targeted imaging and therapy". *Advanced drug delivery reviews* **60**, 1241-51 (2008).

12. Hwang, W., Kim, B., Dandu, R., Cappello, J., Ghandehari, H., Seog, J. "Surface Induced nanofiber growth by self-assembly of a silk-elastin-like protein polymer". *Langmuir : the ACS journal of surfaces and colloids* **25**, 12682-6 (2009).

13. Gustafson, J.A, Ghandehari, H. "Silk-elastinlike protein polymers for matrix-mediated cancer gene therapy". *Advanced drug delivery reviews* **62**, 1509-23 (2010).

14. Teng, W., Cappello, J., Wu, X. "Recombinant silk-elastinlike protein polymer displays elasticity comparable to elastin". *Biomacromolecules* **10**, 3028-36 (2009).

15. Cresce, A. ICNS 2009 Presentation. (2009).

16. Dandu, R., Cresce, A., Briber, R., Dowell, P., Cappello, J., Ghandehari, H. "Silk–elastinlike protein polymer hydrogels: Influence of monomer sequence on physicochemical properties". *Polymer* **50**, 366-374 (2009).

17. Megeed, Z., Cappello, J., Ghandehari, H. "Genetically engineered silk-elastinlike protein polymers for controlled drug delivery". *Advanced drug delivery reviews* **54**, 1075-91 (2002).

18. Greish, K., Araki, K., Li, D., O'Malley, B., Dandu, R., Frandsen, J., Cappello, J., Ghandehari, H. "Silk-elastinlike protein polymer hydrogels for localized adenoviral gene therapy of head and neck tumors". *Biomacromolecules* **10**, 2183-8 (2009).

19. Jain, T.K., Richey, J., Strand, M., Leslie-Pelecky, D., Flask, C., Labhasetwar, V. "Magnetic nanoparticles with dual functional properties: drug delivery and magnetic resonance imaging". *Biomaterials* **29**, 4012-21 (2008).

20. Corchero, J.L., Villaverde, A. "Biomedical applications of distally controlled magnetic nanoparticles". *Trends in biotechnology* **27**, 468-76 (2009).

21. Xie, J., Wang, J., Niu, G., Huang, J., Chen, K., Li, X., Chen, X. "Human serum albumin coated iron oxide nanoparticles for efficient cell labeling". *Chemical communications (Cambridge, England)* **46**, 433-5 (2010).

22. Hoo, C.M., Starostin, N., West, P., Mecartney, M.L. "A comparison of atomic force microscopy (AFM) and dynamic light scattering (DLS) methods to characterize nanoparticle size distributions". *Journal of Nanoparticle Research* **10**, 89-96 (2008).

23. Kokhanovsky, A. *Light Scattering Reviews 4: Single Light Scattering and Radiative Transfer*. 435-441 (Springer: 2009).

24. Glinka C.J., Barker, J.G., Hammouda, B., Krueger, S., Moyer, J.J., Orts, W.J. "The 30 m Small-Angle Neutron Scattering Instruments at the National Institute of Standards and Technology". *Journal of Applied Crystals* **31**, 430 (1998).

25. Mortensen, K. *Neutrons in Soft Matter*. 1-114 (John Wiley & Sons: 2011).

26. Barker, J., Glinka, C.J., Moyer, J.J., Kim, M.H., Drews, A.R., Agamalian, M. "Design and performance of a thermal-neutron double-crystal diffractometer for USANS at NIST". *Journal of Applied Crystals* **38**, 1004 (2005).

27. Cullity, B.D., Graham, C.D. *Introduction to Magnetic Materials*. 67-70 (John Wiley & Sons: 2011).

28. Spaldin, N. *Magnetic Materials: Fundamentals and Applications*. 49-52 (Cambridge University Press: 2010).

29. Gao, W., Sammes, N. *An introduction to electronic and ionic materials*. 357 (World Scientific: 1999).

30. Kline, S.R. "Reduction and Analysis of SANS and USANS Data Using IGOR Pro". *Journal of Applied Crystals* **39**, 895-900 (2006).